3.1 Introduction

Liquid crystal (LC) is a fluid phase of a substance, in which the entire molecule is disordered enough to be classified as a liquid, but maintains varying degrees of order according to the characteristics of the mesogens. Liquid crystal or mesogenic compounds due to their unique flow characteristics of liquid and the optical properties of crystals have a wide range of valuable scientific and technical applications, especially as display devices, organic light-emitting diodes, photoconductors, anisotropic networks, and semiconductors [1-5].

Schiff bases, imine functional groups (CH = N), are widely used as linking groups for rigid base fragments. It provides greater stability and promotes the formation of mesophases, though it produces a core staggered structure [6, 7]. Schiff's base, easy preparation and low cost make it the ideal choice for basic liquid crystal research. Several characteristic compounds with a variety of molecular shapes have been combined with Schiff base functional groups and have shown remarkable mesogenic properties [8-11]. Since the discovery of 4-methoxybenzylidene-4′-butyl aniline (MBBA), which exhibits a nematic mesophase at room temperature, Schiff bases have been frequently studied [12]. A review of the literature shows that liquid crystals with basic Schiff units have been extensively studied and used as linking groups for the production of various types of liquid crystals [8-11, 13].

On the other hand, compounds that combine liquid crystal properties with metal ion properties are an important research goal today and have led to the development of many types of structures, including many metals [14]. They have both disk-like and rod-shaped liquid crystal properties [15]. In addition to the various complex geometries, variable oxidation states, magnetic properties, and redox behavior are further advantages of metallomesogens [16]. Complexation can also cause differences in the mesogenic properties of uncoordinated ligands [15]. The salicylaldimato metal complexes are known for their mesogenic properties, and due to the intramolecular H-bonding and their ability to form coordinate bonds with metal ions, the imine bond is stabilized. There has been considerable work on metallic mesogens [17]. Among other things, copper(II) complexes of Schiff bases are planar or nearly planar around copper atoms and lead to elongated planar compounds suitable for mesogenic properties [17-19]. Synthesized and studied copper (II) metal complexes, showing various smectic, nematic and columnar LC phases [20-24]. Due to the core properties of copper (II) paramagnetism, these metal isomers have amazing chemical and physical properties and have many potential applications [23].

In this study, new homologous series of Schiff base compounds were synthesized, characterized and their liquid crystal properties investigated. Moreover, using these Schiff bases, copper(II) containing metallomesogens were prepared and studied. The relationship between alkyl chain lengths and the behavior of liquid crystals was also examined.

3.2 Experimental

3.2.1 Material

All reagents were purchased from commercial sources and used as received: 2,4-dihydroxybenzaldehyde from TCI; alkyl bromides were purchased from SRL and Spectrochem, Copper(II) acetate hydrate from Spectrochem; 4-aminoacetanilide was purchased from LobaChem. Column chromatography separations were carried out using silica gel (60-120 mesh), purchased from SRL. The purity of the synthesized compounds was checked by using Silica Gel TLC Plate from Merck.

3.2.2 Characterization

The ^1H and ^{13}C spectra were recorded on an AV 400 MHz Bruker FT-NMR spectrometer in $CDCl_3$ solution with tetramethylsilane (TMS) as an internal standard. The mass spectrum was recorded on Water acquity Ultra performance LC with SQ detector. IR spectra were recorded using Bruker alpha FT-IR spectrometer as KBr pellets. The transition temperatures, enthalpies and entropies were investigated by DSC using a PerkinElmer Thermal Analyzer with heating and cooling rate 10 ^oC per minutes. The Leica DM 2500P polarizing optical microscope provided with a Linkam heating stage was used to study thermal behaviour and optical texture of different compounds. Electronic spectra of the compounds in DMF were recorded on an Agilent UV Cary 60 spectrophotometer using a quartz cuvette. The Conduct metric measurements were carried out on EQUIP-TRONIC digital conductometer.

3.3. Synthesis

3.3.1 Synthesis of series-C

3.3.1.1 Synthesis of 2-Hydroxy- 4-n-alkoxy benzaldehye.

2-Hydroxy- 4-n-alkoxy benzaldehye were prepared by following the method described in chapter 2, section 2.3.1.

3.3.1.2 Synthesis of N-(4-((4-n-alkoxy-2-hydroxybenzylidene) amino)phenyl) acetamide.

All the compounds were prepared by following general method.

Dissolve 2-Hydroxy4-n-alkoxybenzaldehyde (n = 2-8, 10, 12, 14, 16, 18, 10 mmol) and 4-aminoacetanilide (10 mmol) in minimal absolute ethanol, a few drops of glacial acetic acid was added and the reaction mixture was refluxed for 4 hours. After cooling, a yellow crystalline compound was isolated. The compound was filtered, washed with cold ethanol and dried in vacuum (**Scheme1**).

N-(4-((4-n-Propyloxy-2-hydroxybenzylidene)amino)phenyl)acetamide (C3)

Yellowish solid; Yield: 68%; ^{1}H NMR (400 MHz , $CDCl_3$, TMS) δ_H 13.85 (s, ArO**H**, 1H), 8.51 (s, -C**H**=N-, 1H), 7.56 (d, Ar**H**, 2H, *J*=8.8 Hz), 7.28-7.22 (m, Ar**H** **&-NH**, 4H), 6.49 (dd, Ar**H**, 2H, *J*=4.4 Hz), 3.98-3.95 (t, -OC$\mathbf{H_2}$$CH_2$-, 2H), 2.21 (s, -C$\mathbf{H_3}$, 3H), 1.86-1.81 (m, -C$\mathbf{H_2}$-, 2H), 1.08-1.04 (t, -$CH_2C\mathbf{H_3}$, 3H) ; IR ($\upsilon_{max}$, cm^{-1}, KBr) : 3473 (υOH), 3278 (υNH), 2970, 2944, 2880 (υ aliphatic C-H), 1623 (υC=O), 1598 (υC=N), 1541, 1507 (υ aromatic C=C), 1195 (υ PhO), 1134 (υ aliphatic C-O).

N-(4-((4-n-Butyloxy-2-hydroxybenzylidene)amino)phenyl)acetamide (C4)

Yellowish solid; Yield: 72%; ^{1}H NMR (400 MHz, $CDCl_3$, TMS) δ_H 13.82 (s, ArO**H**, 1H), 8.53 (s, -C**H**=N-, 1H), 7.56 (d, Ar**H**, 2H, *J*=8.4 Hz), 7.34 (s, **-NH**), 7.28-7.24 (m, Ar**H**, 3H), 6.48 (dd, Ar**H**, 2H, *J*=4.8 Hz), 4.01-4.00 (t, -OC$\mathbf{H_2}$CH_2-, 2H), 2.22 (s, -C$\mathbf{H_3}$, 3H), 1.82-1.48 (m, -C$\mathbf{H_2}$-, 4H), 1.01-1.00 (t, -CH_2C$\mathbf{H_3}$, 3H); IR (υ_{max}, cm^{-1}, KBr): 3507 (υOH), 3325 (υNH), 2979, 2930, 2885 (υ aliphatic C-H), 1666 (υC=O), 1621 (υC=N), 1541, 1515 (υ aromatic C=C), 1190 (υ PhO), 1110 (υ aliphatic C-O).

N-(4-((4-n-Hexyloxy-2-hydroxybenzylidene)amino)phenyl)acetamide (C6)

Yellowish solid; Yield: 70%; Mass (ES): m/z $[M+H]^+$ = 355.32; ^{1}H NMR (400 MHz, $CDCl_3$, TMS) δ_H 13.82 (s, ArO**H**, 1H), 8.52 (s, -C**H**=N-, 1H), 7.56 (d, Ar**H**, 2H, *J*=8.4 Hz), 7.34 (s, **-NH**) 7.28-7.23 (m, Ar**H**, 3H), 6.49 (d, Ar**H**, 2H, *J*=7.8 Hz), 4.02-3.99 (t, -OC$\mathbf{H_2}$CH_2-, 2H), 2.20 (s, -C$\mathbf{H_3}$, 3H), 1.83-1.34 (m, -C$\mathbf{H_2}$-, 8H), 0.95-0.91 (t, -CH_2C$\mathbf{H_3}$, 3H); IR (υ_{max}, cm^{-1}, KBr): 3442 (υOH), 3281 (υNH), 2927, 2872, 2857 (υ aliphatic C-H), 1661 (υC=O), 1627 (υC=N), 1543, 1488 (υ aromatic C=C), 1193 (υ PhO), 1122 (υ aliphatic C-O).

N-(4-((4-n-Heptyloxy-2-hydroxybenzylidene)amino)phenyl)acetamide (C7)

Yellowish solid; Yield: 75%; ^{1}H NMR (400 MHz , $CDCl_3$, TMS) δ_H 13.83 (s, ArO**H**, 1H), 8.52 (s, -C**H**=N-, 1H),7.6 (d, Ar**H**, 2H, *J*=8.4 Hz), 7.43 (s, **-NH**) 7.28-7.32 (m, Ar**H**, 3H), 6.49 (d, Ar**H**, 2H, *J*=6.4 Hz), 4.01-3.99 (t, -OC$\mathbf{H_2}$CH_2-, 2H), 2.22 (s, -C$\mathbf{H_3}$, 3H), 1.83-1.33 (m, -C$\mathbf{H_2}$-, 10H), 0.94-0.91 (t, -CH_2C$\mathbf{H_3}$, 3H); IR (υ_{max}, cm^{-1}, KBr): 3442 (υOH), 3280 (υNH), 2918, 2848 (υ aliphatic C-H), 1661 (υC=O), 1626 (υC=N), 1545, 1472 (υ aromatic C=C), 1196 (υ PhO), 1122 (υ aliphatic C-O).

N-(4-((4-n-Octayloxy-2-hydroxybenzylidene)amino)phenyl)acetamide (C8)

Yellowish solid; Yield: 70%; ^{1}H NMR (400 MHz, $CDCl_3$, TMS) δ_H 13.82 (s, ArO**H**, 1H), 8.54 (s, -C**H**=N-, 1H), 7.58 (d, Ar**H**, 2H, *J*=8.4 Hz), 7.30-7.25 (m, Ar**H & -NH** , 4H), 6.51 (d, Ar**H**, 2H, *J*=8.4 Hz), 4.04-4.01 (t, -OC**H_2**CH_2-, 2H), 2.28 (s, -C**H_3**, 3H), 1.86-1.33 (m, -C**H_2**-, 12H), 0.94-0.91 (t, -CH_2C**H_3**, 3H); IR (υ_{max}, cm^{-1}, KBr): 3281 (υOH), 3281 (υNH), 2954, 2924, 2854 (υ aliphatic C-H), 1661 (υC=O), 1626 (υC=N), 1569, 1543 (υ aromatic C=C), 1194 (υ PhO), 1121 (υ aliphatic C-O).

N-(4-((4-n-Decyloxy-2-hydroxybenzylidene)amino)phenyl)acetamide (C10)

Yellowish solid; Yield: 72%; ^{1}H NMR (400 MHz, $CDCl_3$, TMS) δ_H 13.80 (s, ArO**H,** 1H), 8.53 (s, -C**H**=N-, 1H), 7.56 (d, Ar**H**, 2H, *J*=8.8 Hz), 7.28-7.25 (m, Ar**H & -NH**, 4H), 6.49 (dd, Ar**H,** 2H, *J*=7.2 Hz), 4.02-3.99 (t, -OC**H_2**-, 2H), 2.22 (s, -COC**H_3**, 3H), 1.85-1.29 (m, -C**H_2**-, 16H), 0.91-0.90 (t, -C-C**H_3**, 3H); IR (υ_{max}, cm^{-1}, KBr): 3281 (υOH), 3281 (υNH), 2954, 2918, 2849 (υ aliphatic C-H), 1661 (υC=O), 1626 (υC=N), 1572, 1544 (υ aromatic C=C), 1195 (υ PhO), 1122 (υ aliphatic C-O).

N-(4-((4-n-Dodecyloxy-2-hydroxybenzylidene)amino)phenyl)acetamide (C12)

Yellowish solid; Yield: 76%; ^{1}H NMR (400 MHz, $CDCl_3$, TMS) δ_H 13.81 (s, ArO**H,** 1H), 8.53 (s, -C**H**=N-, 1H), 7.56 (d, Ar**H**, 2H, *J*=8.8 Hz), 7.28-7.25 (m, Ar**H & -NH**, 4H), 6.49 (d, Ar**H,** 2H, *J*=7.8 Hz), 4.02-3.99 (t, -OC**H_2**-, 2H), 2.22 (s, -COC**H_3**, 3H), 1.84-1.28 (m, -C**H_2**-, 20H), 0.91-0.88 (t, -C-C**H_3**, 3H); IR (υ_{max}, cm^{-1}, KBr): 3440 (υOH), 3281 (υNH), 2919, 2849 (υ aliphatic C-H), 1661 (υC=O), 1626 (υC=N), 1545 (υ aromatic C=C), 1195 (υ PhO), 1122 (υ aliphatic C-O).

N-(4-((4-n-Tetradecyloxy-2-hydroxybenzylidene)amino)phenyl)acetamide (C14)

Yellowish solid; Yield: 68%; ^{1}H NMR (400 MHz, $CDCl_3$, TMS) δ_H 13.80 (s, ArO**H,** 1H), 8.53 (s, -C**H**=N-, 1H), 7.56 (d, Ar**H**, 2H, *J*=7.6 Hz), 7.28-7.24 (m, Ar**H & -NH**, 4H), 6.49 (d, Ar**H** 2H, *J*=7.2 Hz), 4.02-3.99 (t, -OC$\mathbf{H_2}$-, 2H), 2.22 (s, -COC$\mathbf{H_3}$, 3H), 1.82-1.27 (m, -C$\mathbf{H_2}$-, 24H), 0.91-0.88 (t, -C-C$\mathbf{H_3}$, 3H); IR (υ_{max}, cm^{-1}, KBr): 3441 (υOH), 3280 (υNH), 2918, 2849 (υ aliphatic C-H), 1661 (υC=O), 1625 (υC=N), 1571, 1545 (υ aromatic C=C), 1195 (υ PhO), 1122 (υ aliphatic C-O).

N-(4-((4-n-Hexadecyloxy-2-hydroxybenzylidene)amino)phenyl)acetamide (C16)

Yellowish solid; Yield: 75%; ^{1}H NMR (400 MHz, $CDCl_3$, TMS) δ_H: 13.79 (s, ArO**H,** 1H), 8.55 (s, -C**H**=N-, 1H), 7.58 (d, Ar**H**, 2H, *J*=8.8 Hz), 7.30-7.24 (m, Ar**H & -NH**, 4H), 6.52 (dd, Ar**H**, 2H, *J*=8.8 Hz), 4.05-4.02 (t, -OC$\mathbf{H_2}$$CH_2$-, 2H), 2.24 (s, -COC$\mathbf{H_3}$, 3H), 1.85-1.24 (m, -C$\mathbf{H_2}$-, 28H), 0.93-0.90 (t, -$CH_2C\mathbf{H_3}$, 3H); IR ($\upsilon_{max}$, cm^{-1}, KBr): 3441 (υOH), 3281 (υNH), 2918, 2849 (υ aliphatic C-H), 1661 (υC=O), 1625 (υC=N), 1571, 1545 (υ aromatic C=C), 1195 (υ PhO), 1122 (υ aliphatic C-O).

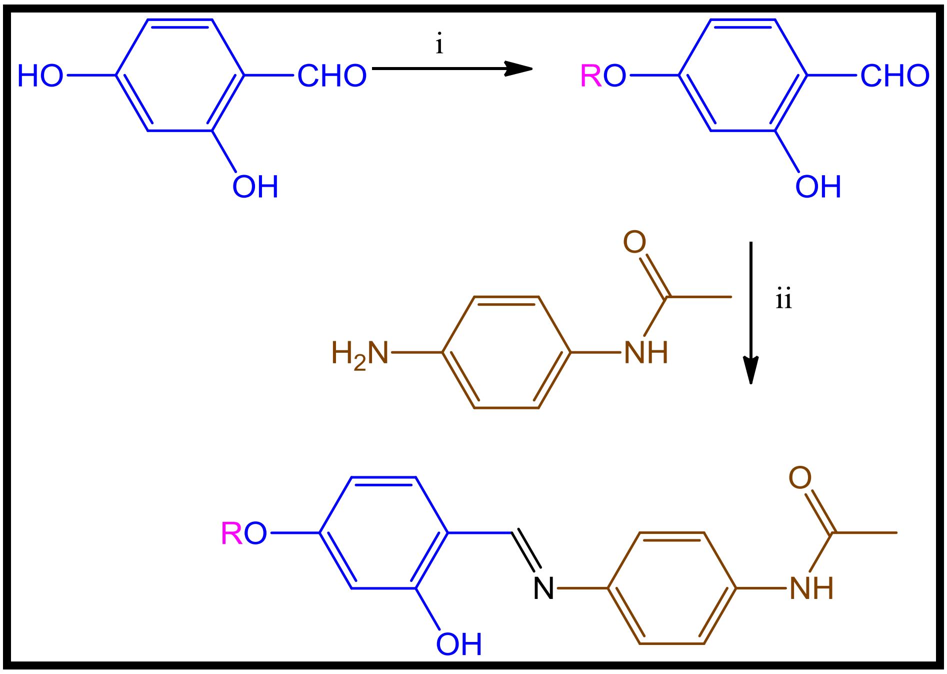

Where R = C_nH_{2n+1}; n = 2 to 8, 10, 12, 14, 16, 18.

i) RBr, $KHCO_3$, KI, dry acetone, reflux 24 hrs

ii) Glacial AcOH, absolute EtOH, reflux 4 hrs

Scheme1. Synthesis protocol of series C

3.3.2 Synthesis of series D

3.3.2.1 Synthesis of Cu(II) complexes

The Cu(II) complex was prepared by the following the general method.

Dissolve hydrated copper (II) acetate (2 mmol) in a minimum amount of ethanol, and add this solution to the hot ethanol solution of the ligand (n = 2- 8, 10, 12, 14, 16, 18, 4 mmol). The reaction mixture was refluxed for 4 hours, during which a crystalline solid formed, which was filtered off, washed with hot distilled water, then washed with ethanol and dried under vacuum (Scheme 2).

Bis(2-((E)-((4-acetylphenyl)imino)methyl)-5-butyloxy)phenoxy)copper (D4)

Brownish solid; Yield: 68%; IR (υ_{max}, cm^{-1}, KBr): 3297 (υ NH), 2919, 2850 (υ aliphatic C-H), 1657 (υC=O), 1611 (υC=N), 1589, 1522 (υ aromatic C=C), 1205 (υ PhO), 1127 (υ aliphatic C-O), 591 (υM-N), 531 (υM-O).

Bis(2-((E)-((4-acetylphenyl)imino)methyl)-5-(hexyloxy)phenoxy)copper (D6)

Brownish solid; Yield: 65%; Mass (ES): m/z $[M+2]^+$ = 765.51 IR (υ_{max}, cm^{-1}, KBr): 3304 (υ NH), 2930, 2868 (υ aliphatic C-H), 1681 (υC=O), 1611 (υC=N), 1586, 1506 (υ aromatic C=C), 1188 (υ PhO), 1122 (υ aliphatic C-O), 589 (υM-N), 536 (υM-O).

Bis(2-((E)-((4-acetylphenyl)imino)methyl)-5-(heptyloxy)phenoxy)copper (D7)

Brownish solid; Yield: 68%; IR (υ_{max}, cm^{-1}, KBr): 3302 (υ NH), 2927, 2855 (υ aliphatic C-H), 1669 (υC=O), 1611 (υC=N), 1587, 1506 (υ aromatic C=C), 1190 (υ PhO), 1122 (υ aliphatic C-O), 591 (υM-N), 537 (υM-O).

Bis(2-((E)-((4-acetylphenyl)imino)methyl)-5-(octayloxy)phenoxy)copper (D8)

Brownish solid; Yield: 75%; IR (υ_{max}, cm^{-1}, KBr): 3296 (υ NH), 2924, 2853 (υ aliphatic C-H), 1658 (υC=O), 1609 (υC=N), 1588, 1522 (υ aromatic C=C), 1191 (υ PhO), 1125 (υ aliphatic C-O), 590 (υM-N), 540 (υM-O); Conductance: 10 $ohm^{-1}cm^2mol^{-1}$

Bis(2-((E)-((4-acetamidophenyl)imino)methyl)-5-decyloxyphenoxy)copper (D10)

Brownish solid; Yield: 82%; IR (υ_{max}, cm^{-1}, KBr): 3296 (υ NH) 2920, 2851 (υ aliphatic C-H), 1657 (υC=O), 1610 (υC=N), 1588, 1521 (υ aromatic C=C), 1205, 1191 (υ PhO), 1125 (υ aliphatic C-O), 590 (υM-N), 541 (υM-O).

Bis(2-((E)-((4-acetamidophenyl)imino)methyl)-5-dodecyloxyphenoxy)copper (D12)

Brownish solid; Yield: 74%; IR (υ_{max}, cm^{-1}, KBr): 3297 (υ NH) 2920, 2851 (υ aliphatic C-H), 1657 (υC=O), 1610 (υC=N), 1589, 1522 (υ aromatic C=C), 1206 (υ PhO), 1126 (υ aliphatic C-O), 591(υM-N), 542(υM-O).

Bis(2-((E)-((4-acetamidophenyl)imino)methyl)-5-tetradecyloxyphenolxy) copper (D14)

Brownish solid; Yield: 82%; IR (υ_{max}, cm^{-1}, KBr): 3297 (υ NH), 2920, 2851 (υ aliphatic C-H), 1657 (υC=O), 1610 (υC=N), 1589, 1521 (υ aromatic C=C), 1205, 1192 (υ PhO), 1126 (υ aliphatic C-O), 591 (υM-N), 542 (υM-O); Conductance: 6 $ohm^{-1}cm^{2}mol^{-1}$

Bis(2-((E)-((4-acetamidophenyl)imino)methyl)-5-hexadecyloxyphenoxy) copper (D16)

Brownish solid; Yield: 80%; IR (υ_{max}, cm^{-1}, KBr): 3297 (υ NH), 2920, 2850 (υ aliphatic C-H), 1657 (υC=O), 1610 (υC=N), 1589, 1510 (υ aromatic C=C), 1204, 1191 (υ PhO), 1126 (υ aliphatic C-O), 590 (υM-N), 541 (υM-O).

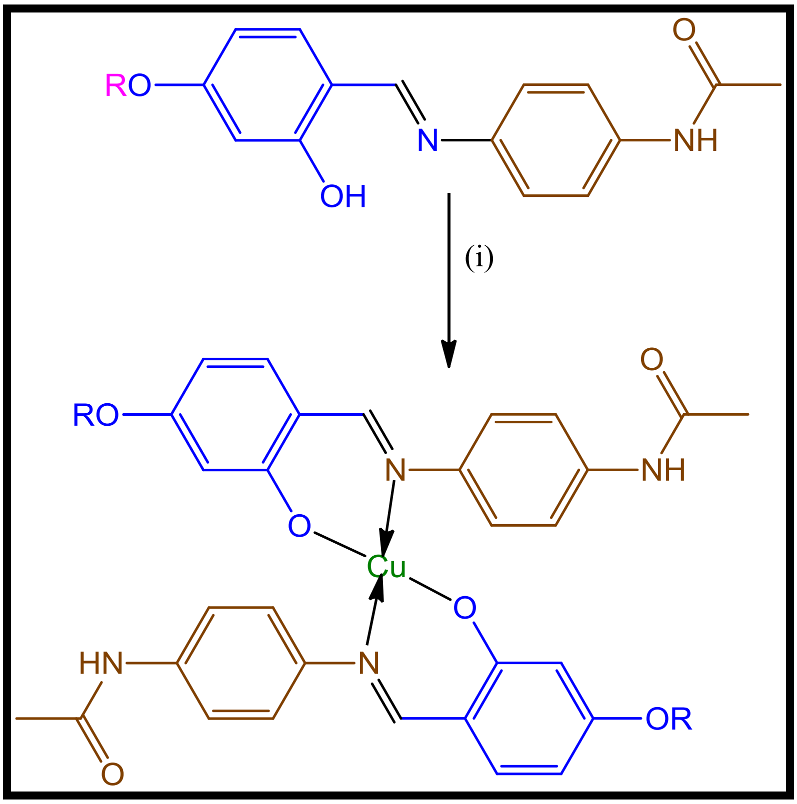

Where R = C_nH_{2n+1}; n = 2 to 8, 10, 12, 14, 16, 18.

i) $Cu(COOCH_3)_2.H_2O$, absolute EtOH, reflux 3 hrs.

Scheme 2. Synthetic protocol of Cu(II) complexes.

3.4 Results and discussion

3.4.1 Series-C

In this series, 12 new homologous of N-(4-((4-n-Alkoxy-2-hydroxybenzylidene) amino)phenyl)acetamide were synthesized and characterized by FT-IT and ^{1}H-NMR spectroscopy. The ^{1}H-NMR spectrum of series-A, shows the following characteristic absorptions which confirm the synthesized compounds. The hydroxyl proton (–OH) of Schiff base is observed in as a singlet around δ 13.82. This proton was observed deshielded, due to the presence of intramolecular hydrogen bonding between the hydroxyl group and the imine group. The proton of the imine group (-CH=N-) around δ 8.53 is appeared as a singlet. In some synthesized Schiff bases, the –NH proton was observed at δ 7.43-7.34 as a singlet and in some of them merged with aromatic protons. The aromatic ring protons are observed between δ 7.32-6.48. The methylene protons (-CH_2O-) attached to oxygen are obtained as triplets between δ 4.05-3.95. The methyl proton, attached with carbonyl group (-$COCH_3$),is observed at δ 2.28-2.20 as a singlet for all the synthesized Schiff bases. The -CH_2- units in alkoxy chain were observed in between δ 1.85-1.24 as a multiplet and the terminal -CH_3 group protons of alkoxy chain were observed in between δ 1.08-0.88 as a triplet. The ESI-Mass spectra of one of the homolog **C6** $[M + H]^+$ peak obtained at m/z 355.32 confirmed the structure of the molecule.

In the FT-IR spectrum, the characteristic peak of carbonyl stretching was observed at approximately 1661 cm^{-1} for all compounds in the series. In the compounds absorption band around 1627-1621 cm^{-1} is attributed to imine linkage (υC=N).

The mesomorphic properties of all synthesized compounds were investigated using differential scanning calorimetry (DSC) and polarising optical microscope (POM). The phase transition temperatures in ^{o}C, associated transition enthalpy values (ΔH Jg^{-1}) are presented in **Table 1**. POM images of **C7** and **C14** compounds are shown in **Figure 1.**

Series-C		
Cn	**Heating**	**Cooling**
C2	Cr 209.1 I	I 190.3Cr
C3	Cr 190.6 I	I 171.8 Cr
C4	Cr 180.2 I	I165.3 Cr
C5	Cr 154.3(16.49) I	I 138.8(35.95) Cr
C6	Cr 145.0(0.36)SmA167.0(21.59) I	I 150.4(0.95) SmA 134.7(2.65) Cr
C7	Cr 57.8(7.32) Cr' 152.2(15.17)SmA 169.7(1.03) I	I 164.1(0.95) SmA 135.7(5.31) Cr' 43.4(2.28)Cr
C8	Cr 50.8(3.42) Cr'153.6(17.04)SmA 183.9(0.82) I	I 178.5(1.23) SmA 132.1(3.63) Cr
C10	Cr 81.3(4.68) Cr'149.4(13.24)SmA193.2(2.77)Cr	I 189.3(1.24) SmA 125.4(0.52) Cr'69.4(1.30)Cr
C12	Cr 98.7(7.37) Cr'144.6(17.82)SmA195.7(2.26)Cr	I 190.4(2.08) SmA 123.8(39.65) Cr'84.5(4.33)Cr
C14	Cr 108.9(6.35) Cr'141.0(12.68)SmA196.3(0.49)Cr	I 190.9(0.64) SmA 121.6(14.68) Cr'92.14(3.40)Cr
C16	Cr 113.8(8.61) Cr'138.8(9.71)SmA196.7(1.87)Cr	I 191.1(1.29) SmA 120.5(4.71) Cr'101.6(10.09)Cr
C18	Cr 117.3(4.18) Cr' 137.3(7.81) SmA 193.9(1.81) I	I 186.7(1.24) SmA 118.2(1.90) Cr'103.6(3.86)Cr

Table 1. Phase transition temperatures in ^{o}C, associated transition enthalpy values (ΔH Jg^{-1}).

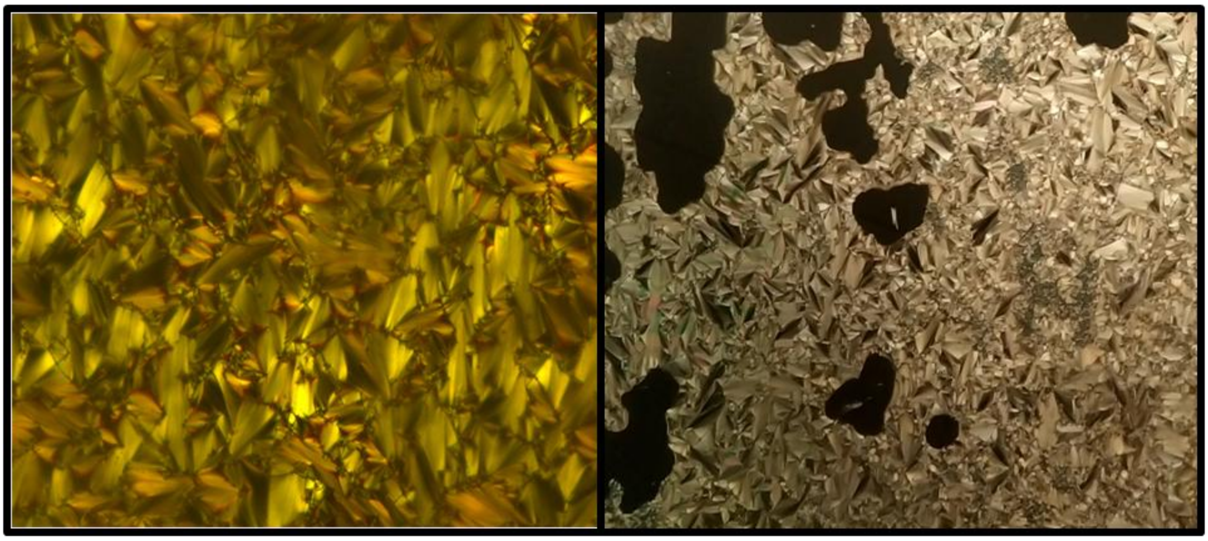

(a) (b)

Figure 1. Fan-like texture of SmA phase (a) **C7** on cooling at 160.1 ^{o}C (b) **C12** on heating at 192.6 ^{o}C

The thermal results of compounds show that up to *n*-pentyloxy derivatives are non-mesogenic due to lack of suitable end to end and lateral intermolecular attraction which under exposed to thermal vibrations obstruct to molecules in their floating condition to maintain sliding moving layer [25]. The **C5** DSC thermogram show endothermic peak at 154.3^{o}C, corresponding to Cr to I, and exothermic peak at 138.8^{o}C which is related to I to Cr transition (**Figure 2**).This confirm the non-mesomorphic behaviour of **C5.** Then all the members of the series, from *n*-hexyloxy to *n*-octadecyl oxy, melt between 137-154 ^{o}C, depending on the length of the alkyl chain. Under the polarizing optical microscope the fluids display typical fan shape optical texture of SmA phase. They show mesomorphic behavior due to the resultant molecular rigidity and flexibility generates appropriate magnitudes of anisotropic forces of intermolecular end to end and lateral attractions. The DSC thermogram of **C7** shows three endothermic peaks at 57.8^{o}C, 152.2^{o}C and 169.7 ^{o}C, followed by three exothermic peaks at 164.1 ^{o}C,135.7 ^{o}C and 43.4 ^{o}C. The endothermic peaks are related to Cr to Cr', Cr' to SmA phase and SmA phase to I transitions, while the exothermic peaks are attributed to I to SmA phase, SmA phase to Cr' and Cr' to Cr transitions. In the DSC thermogram of **C12** , three endothermic peaks at 98.7 ^{o}C, 144.6 ^{o}C and 95.7 ^{o}C are observed. They correspond to transitions from Cr to Cr', Cr' to SmA and SmA to I. Three exothermic peaks were observed at 190.4 ^{o}C, 123.8 ^{o}C and 84.5 ^{o}C corresponding to the transition of I to SmA, SmA to Cr' and Cr' to Cr (**Figure 2**). In the series, we observe that enthalpy changes for Cr in SmA is higher (ΔH= ~7-18 Jg^{-1}) than the SmA transition in I (ΔH= ~3-1 Jg^{-1}).

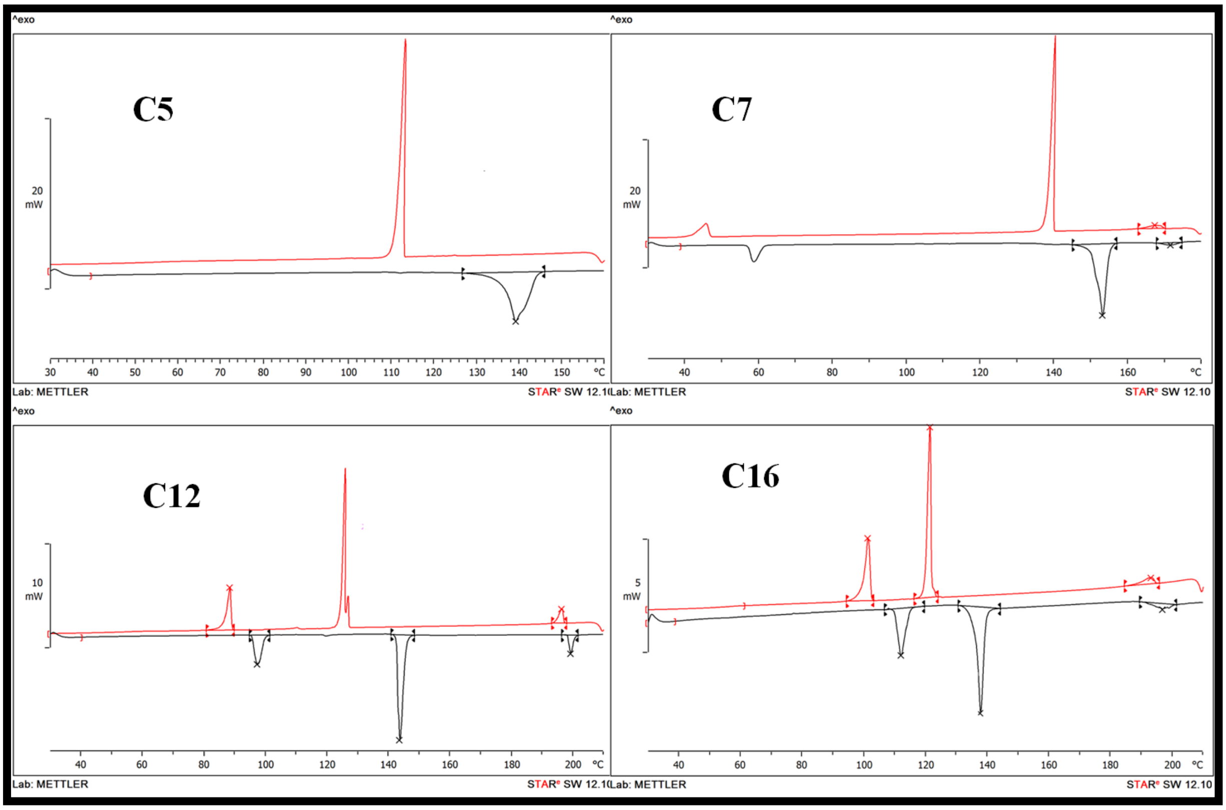

Figure 2. DSC thermogrames of Schiff base.

The obtained transition temperature is plotted against the number of carbon atoms, as shown in **Figure 3**. The transition temperature follows the decreasing trend of Cr to SmA transition as the length of the terminal alkoxy chain increases. The long alkoxy group in the end may reduce the van der Waals interactions between the phenylaromatic nuclei. The degree of flexibility increases, leading to a decrease in the transition temperature [26]. The clearing temperature increases, as the terminal alkoxy chain increases up to the *n*-hexadecyloxy group (-$OC_{16}H_{33}$); then in the *n*-octadecyloxy group (-$O_{18}H_{37}$) decreases.

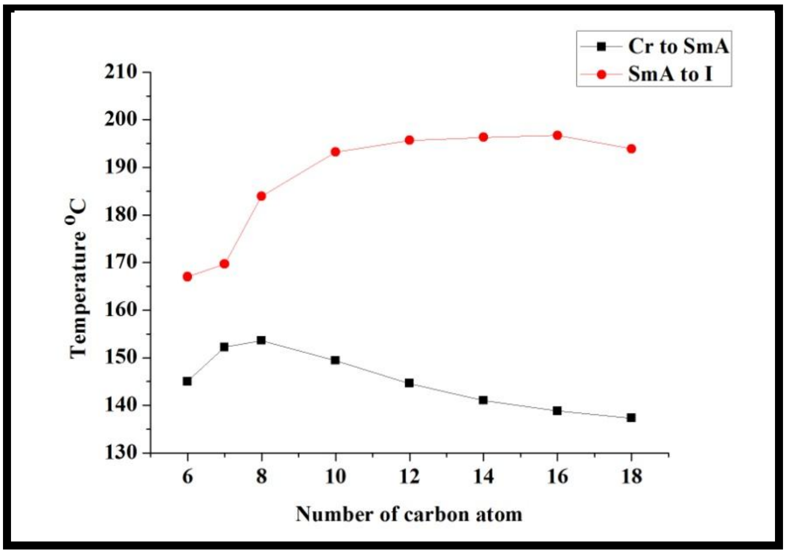

Figure3. Dependence of transition temperatures on the increasing terminal alkoxy chain length

For the series, smectic-A phase temperature range is plotted as a function of the increase in chain length during the cooling and heating cycles, as shown in **Figure 4**. Due to super cooling effect, all compounds show a higher SmA phase range on cooling compared to heating. In the series, the compound with *n*-hexadecyloxy ($-OC_{16}H_{33}$) chain length shows the highest temperature range of SmA phase.

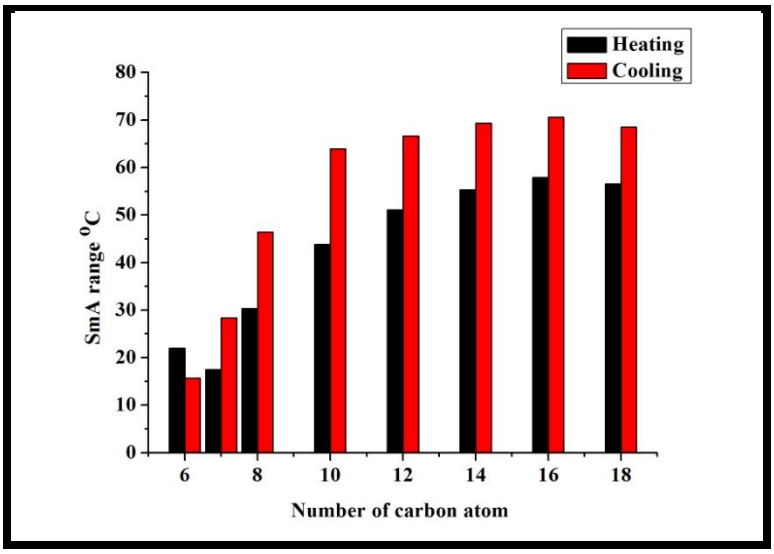

Figure4. Temperature range of SmA phase transition

3.4.2 Series-D

In this series, twelve new homologous, Cu (II) complexes of N-(4-((4-n-Alkoxy-2-hydroxybenzylidene)amino)phenyl)acetamide were synthesized and well characterized by FT-IR. In the FT-IR spectrum, the typical peak of carbonyl stretching was observed around 1658 cm^{-1} all compounds in the series. The metal complexes exhibits bands around 16011-1609 cm^{-1}, corresponding to (υC=N). The lowering of the peak of (υC=N) in metal complexes is compared to the ligand indicating the formation of complex through N of the azomethine group. The metal complexes exhibited the peaks around 591-589 cm^{-1} and 542-537 cm^{-1} due to (υM-N) and (υM-O) vibrations.

The electronic spectra of free ligands (**C6** and **C14**) and related copper complexes (**D6** and **D14**) in DMF from 280 to 480 nm are depicted in **Figure 5**. Electronic spectra of free ligands display band at 355 nm is attributed to $\pi \rightarrow \pi^*$ transition. The λ_{max} of free ligands in copper complexes is red shifted to 365 nm. The bathochromic effect seen for the copper complexes arises due to the chelation by copper. The electronic spectra of Cu(II) complexes show an absorption band at 660-680 nm attributed to the dxy → dx^2-y^2 transition. The conductance values of complexes (section 3.3.2.1) clearly indicate their non-electrolyte behavior. The mass spectra of the **D6** (section 3.3.2.1) indicates the ML_2 type of complex, which are compatible with these complexes having square-planar structure.

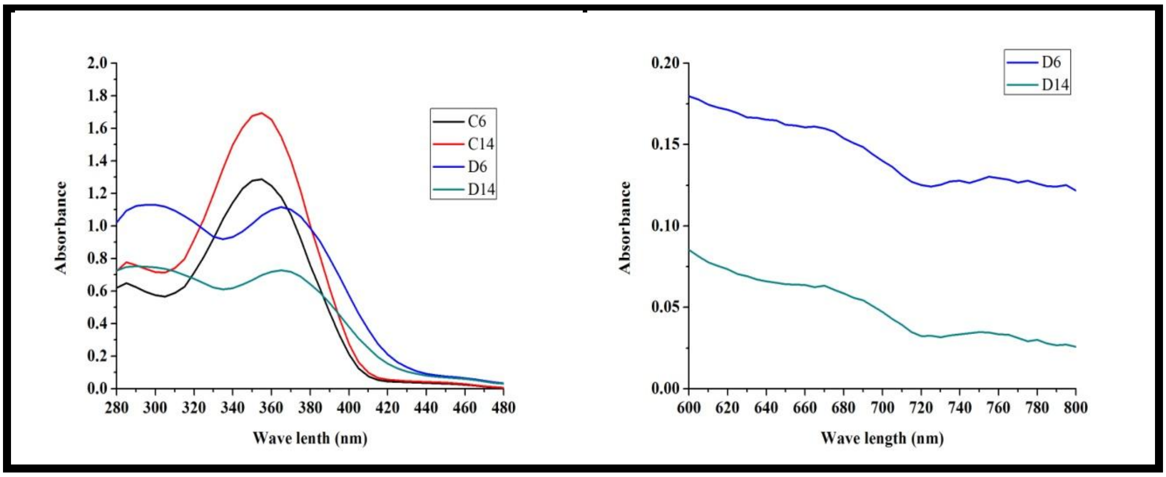

Figure 5. Electronic spectra of ligands and complexes

The mesomorphic properties of all synthesized compounds were studied by differential scanning calorimetry (DSC) and polarizing optical microscope (PMO).The phase transition temperatures in ^{o}C, associated transition enthalpy values (ΔH Jg^{-1}) are listed in **Table.2** The POM images of compound **D8** and **D18** are as shown **Figure 6**.

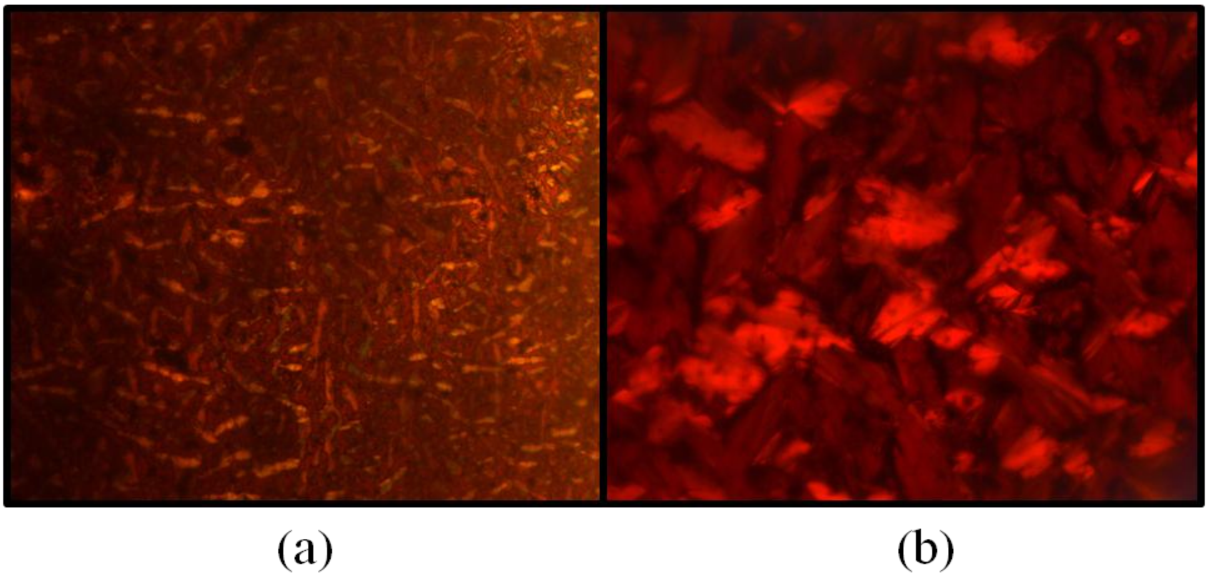

Figure 6. Fan-like texture of SmA phase (a) **D8** on cooling at 230.3 ^{o}C (b) **D18** on cooling at 235.7 ^{o}C

Series-D

Dn	Heating	Cooling
D2	Cr >300I	-
D3	Cr>300I	-
D4	Cr >300 I	-
D5	Cr 290.2 I	I 170Cr
D6	Cr 271.0 I	I 185.3Cr
D7	Cr 250.4 I	I 175.0 Cr
D8	Cr 221.1(9.75)SmA 236.7(24.10) I	I 230.3 SmA 212.5 Cr
D10	Cr 213.1 SmA 245.3 I	I 222.8 SmA 167.6 Cr
D12	Cr 213.2 SmA 250.6 I	I223.5 SmA166.3Cr
D14	Cr 208.3 SmA 265.8 I	I242.7 SmA 165.2 Cr
D16	Cr 204.5 SmA 260.3 I	I223.8 SmA155.2 Cr
D18	Cr 220.3 SmA 254.6 I	I240.7 SmA170.6Cr

Table2. Phase transition temperatures in ^{o}C, associated transition enthalpy values (ΔH Jg^{-1}). Where n = no. of carbon atom in alkoxyl chain; Cr & Cr’ = Crystal; SmA = SmecticA and I = Isotropic

The thermal results of the complexes show that from *n*-ethoxy to *n*-hexyloxy derivatives melts directly from the crystalline phase to the isotropic liquid without exhibiting an intermediate phase. While *n*-octyloxy to *n*-octadecyloxy shows an enantiotropic smectic-A phase behaviour. The DSC thermogram of **D8** show two endothermic peaks at 221.1^{o}C and 236.7^{o}C which is corresponding to Cr to SmA and SmA to I transitions respectively, while on cooling it does not show any peak **(Figure 7).**

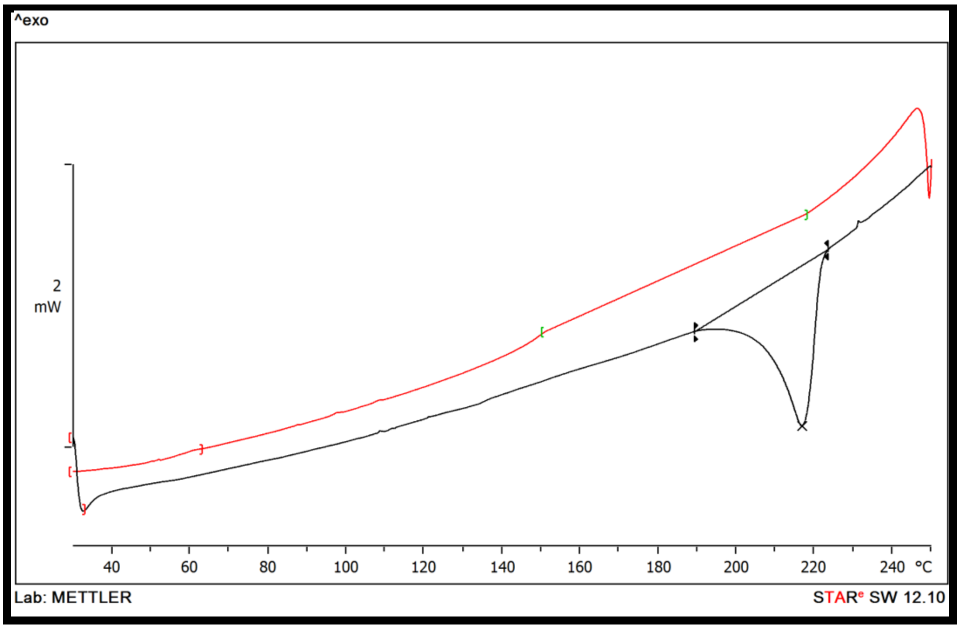

Figure 7.DSC thermogrames of complex **D8**.

The obtained transition temperatures as a function of number of carbon atom were plotted, shown **Figure 8**. The result indicates that Cr to SmA transition temperatures are not found in order in this series. Whereas the clearing temperature increases with the increase of the terminal alkoxy group to the *n*-tetradecyloxy group (-OC14H29) and then after the decrease.

For the synthesized series, smectic-A phase temperature range as function of increasing chain length in the cooling and heating cycle were plotted, shown in **Figure 9**. All the compounds show higher SmA phase range on cooling compare to heating which is due to super cooling effect. In the series of complex compound with n-tetradecyloxy (-$OC_{14}H_{29}$) chain length shows the maximum temperature range of SmA phase.

For the synthesized Schiff base ligand, the SmA mesophase appears in the range of 135-200°C, while in its Cu complex, it appears in the range of 205-270°C. This clearly shows that the presence of metallic copper stabilizes the mesophase at higher temperatures.

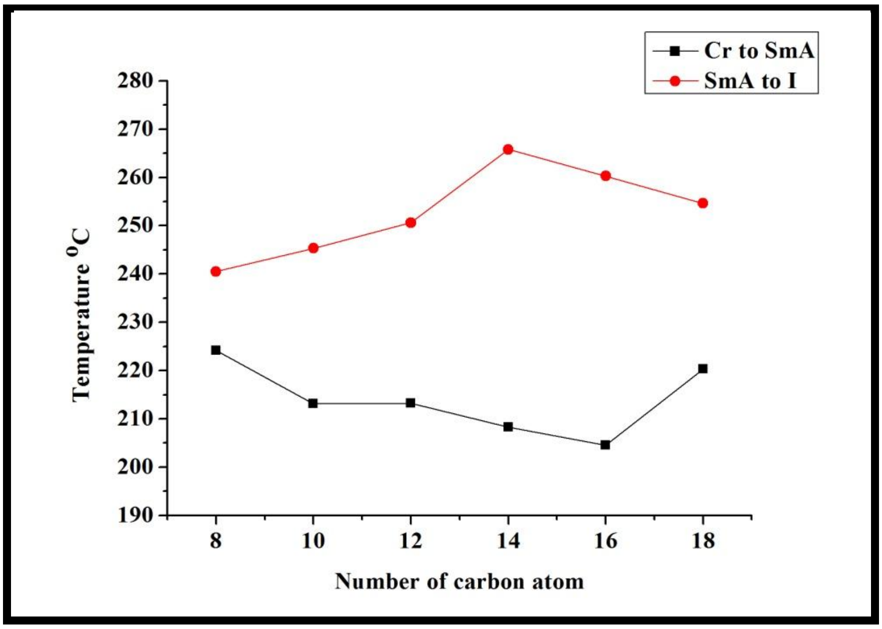

Figure 8. Dependence of transition temperatures on the increasing terminal alkoxy chain length

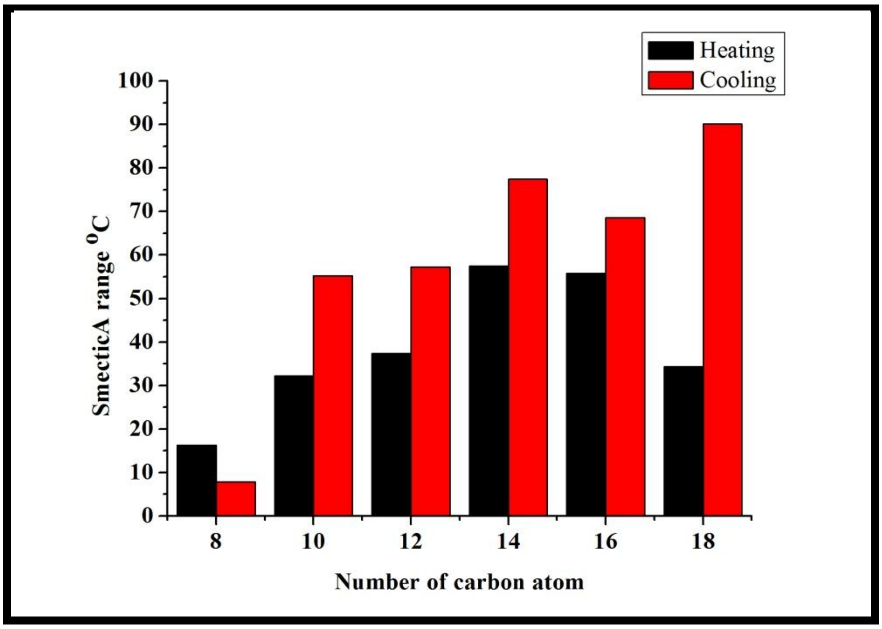

Figure 9.Temperature range of SmA phase transition

3.5 Structurally similar compounds.

Comparing the mesogenic behavior of the homologous series C with series A, and series D with series B, from chapter 2, the structure is similar; as shown in **Figure 10**.The series C and series A chosen for comparison are structurally identical with respect to two phenyl rings linked through –CH=N– central bridge that contribute to molecular rigidity and the left alkoxy terminal end group that contributes to the molecular flexibility. In series A mesophase commence from n-propoxy, and it was the monotropic SmA while in series C mesophase commence from n-hexayloxy, and it was the enantiotropic SmA. In series B mesophase commence from n-pentyloxy, and it was the monotropic SmA while in series D mesophase commence from n-octyloxy, and it was the enantiotropic SmA. The higher homologous in the all the series exhibited enantiotropic SmA phase. It was observed that the SmA mesophase thermal stability of compound series C is higher than that of series A. Similarly the SmA mesophase thermal stability of series D is higher than for series B. Difference in terminal tail end functional groups–$NHCOCH_3$ and –$COCH_3$ whose polarity and polarizability creates difference in the magnitudes of mesomorphism and the degree of mesomorphism [27].

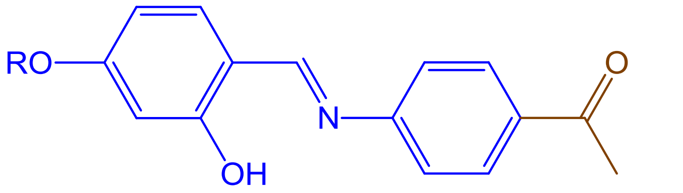

Series A

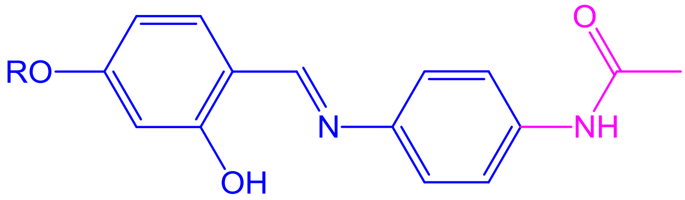

Series C

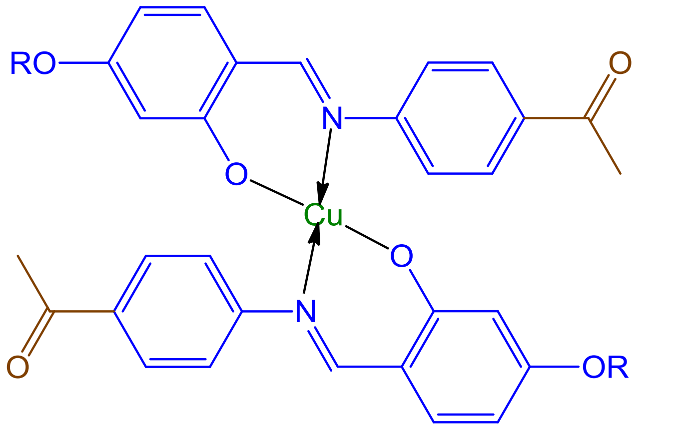

Series B

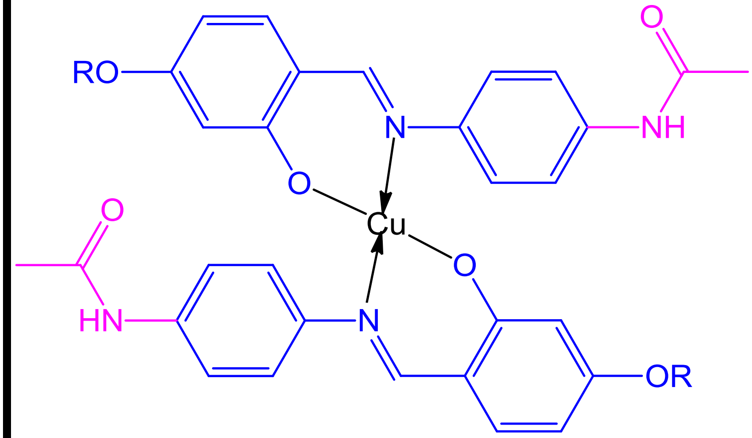

Series D

Figure 10. Structurally similar compounds

3.6 Conclusion

In the present work, two homologues series of Schiff base ligand and corresponding Cu(II) complex have been synthesized and well characterized by FT-IR and ^{1}H-NMR measurements. All the mesophases observed were confirmed by the optical textural observation under POM and DSC thermogram studies. Both the series exhibited enantiotropic smectic A phase, in the homologues series of ligands and Cu(II) metal complexes mesomorphic property commence from n-hexyloxy($-OC_6H_{13}$) terminal end group and n-octyloxy($-OC_8H_{17}$) terminal end group respectively. The clearing temperatures of Cu(II) complexes are higher than the corresponding un co-ordinated ligands due to the presence of metal. It was also observed that mesomorphic behaviour and mesomorphic temperature range be governed by the terminal alkoxy chain length.

3.7 References

[1] Hikmet RAM, Broer DJ. Dynamic mechanical properties of anisotropic networks formed by liquid crystalline acrylates. Polymer. 1991;32:1627–1632.

[2] Chen H-W, Lee J-H, Lin B-Y, et al. Liquid crystal display and organic light-emitting diode display: present status and future perspectives. Light Sci. Appl. 2018;7:17168.

[3] Zhulai D, Koval'chuk A, Bugaychuk S, et al. Photoconductivity of ionic thermotropic liquid crystal with semiconductor nanoparticles. J. Mol. Liq. 2018;267:406–410.

[4] Han MJ, Wei D, Kim YH, et al. Highly oriented liquid crystal semiconductor for organic field-effect transistors. ACS Cent. Sci. 2018;4:1495–1502.

[5] Melnyk O, Garbovskiy Y, Glushchenko A. Science and technology of stressed liquid crystals: display and non-display applications. Phase Transitions. 2017;90:773–779.

[6] Jber N, M. Shukur M, Al Ahmed A. Schiff base liquid crystals with terminal alkoxy group synthesis and thermotropic properties. J. Al-Nahrain Univ. Sci. 2014;17 (2):46-22.

[7] Hagar M, Ahmed HA, Saad GR. Mesophase stability of new Schiff base ester liquid crystals with different polar substituents. Liq. Cryst. 2018;45:1324–1332.

[8] Ha S-T, Koh T-M, Yeap G-Y, et al. Mesogenic Schiff base esters with benzothiazole core: synthesis and phase transition studies. Phase Transitions. 2010;83:195–204.

[9] Ha S-T, Ong L-K, Wong JP-W, et al. Mesogenic Schiff's base ether with dimethylamino end group. Phase Transitions. 2009;82:387–397.

[10] Kala ALA, Harohally N V., Naveen S, et al. o-Hydroxy Schiff bases derived from 2-hydroxy-4-methoxy benzaldehyde: synthesis, x-ray studies and hydrogen bonding attributes. Mol. Cryst. Liq. Cryst. 2016;629:146–157.

[11] Sharma VS, Patel RB. Design and investigation of calamatic liquid crystals: Schiff

base (–CH=N), chalcone (–CO–CH=CH–), and ester (–COO–) linkage group contain rigid rod shape with various terminal parts. Mol. Cryst. Liq. Cryst. 2017;643:141–158.

[12] Hagar M, Ahmed HA, Alhaddad OA. New azobenzene-based natural fatty acid liquid crystals with low melting point: synthesis, DFT calculations and binary mixtures. Liq. Cryst. 2019;46:2223-2234.

[13] Tandel RC, Patel NK. Synthesis and study of liquid crystalline properties of schiff's bases having 1,3,4-thiadiazole moiety. Liq. Cryst. 2014;41:495–502.

[14] Date RW, Bruce DW. Discotic salicylaldimato metal complexes exhibiting columnar mesophases and their mixtures with rod-like salicylaldimato complexes. Liq. Cryst. 2004;31:1435–1444.

[15] Giroud-Godquin A-M, Maitlis PM. Metallomesogens: Metal Complexes in organized fluid phases. Angew. Chemie Int. Ed. English . 1991;30:375–402.

[16] Marcos M, Omenat A, Barberá J, et al. Structural study of metallomesogens derived from tris-[2-(salicylideneamino)ethyl]amine. A molecular meccano. J. Mater. Chem. 2004;14:3321–3327.

[17] Hoshino N. Liquid crystal properties of metal–salicylaldimine complexes.: Chemical modifications towards lower symmetry. Coord. Chem. Rev. 1998;174:77–108.

[18] Datta C, Chakrabarty R, Das G, et al. Influence of spacer group substituent on mesomorphism in copper complexes of 'salen' type Schiff bases bearing long alkoxy arm. Liq. Cryst. 2014;41:541–551.

[19] Nejati K, Rezvani Z, Alizadeh E, et al. Synthesis and mesomorphic properties of symmetric tetradentate Schiff bases based on azo-containing salicylaldimines and their copper(II) complexes. J. Coord. Chem. 2011;64:1859–1870.

[20] Caruso U, Roviello A, Sirigu A. Nematic and smectic mesophases in a new series of

Cu(II) organometallic complexes. Liq. Cryst. 1990;7:421–430.

[21] Heng BT, Yeap GY, Mahmood WAK, et al. New heterocyclic metallomesogens: synthesis, mesomorphic and thermal behaviours of Cu(II) complexes with 1,2,3-triazole-based Schiff bases ligands. Liq. Cryst. 2015;42:204–215.

[22] Cretu C, Cseh L, Tang BJ, et al. Mononuclear Cu(II) complexes of novel salicylidene Schiff bases: synthesis and mesogenic properties. Liq. Cryst. 2015;42:1139–1147.

[23] Thaker BT, Solanki DB, Patel BS, et al. Synthesis, characterisation and liquid crystalline properties of some Schiff base and cinnamate central linkages involving 1,3,5-trisubstituted pyrazolone ring system and their Cu(II) complexes. Liq. Cryst. 2013;40:1296–1309.

[24] Prajapati AK, Bonde N. Synthesis of two naphthyl-containing homologous series of mesogenic ligands and the related metallomesogens containing Cu(II). Liq. Cryst. 2006;33:1189–1197.

[25] Sharma VS, Patel RB. Study the effects of terminal side chain and –nitro group on mesomorphic behaviour of cinnamate-chalconyl based liquid crystal. Mol. Cryst. Liq. Cryst. 2017;643:1–12.

[26] Jadeja UH, Sharma VS, Prajapat V, et al. Synthesis and study of azo based liquid crystals: effect of the lateral bromo and terminal alkoxy side chain on thermal, mesomorphic and optical properties. Mol. Cryst. Liq. Cryst. 2019;680:46–6.

[27] Marcos M, Meléndez E, Ros MB, et al. Influence of Polar End Groups on Induced Smectic Phase Appearance. Mol. Cryst. Liq. Cryst. Inc. Nonlinear Opt. 1989;167:239–252.

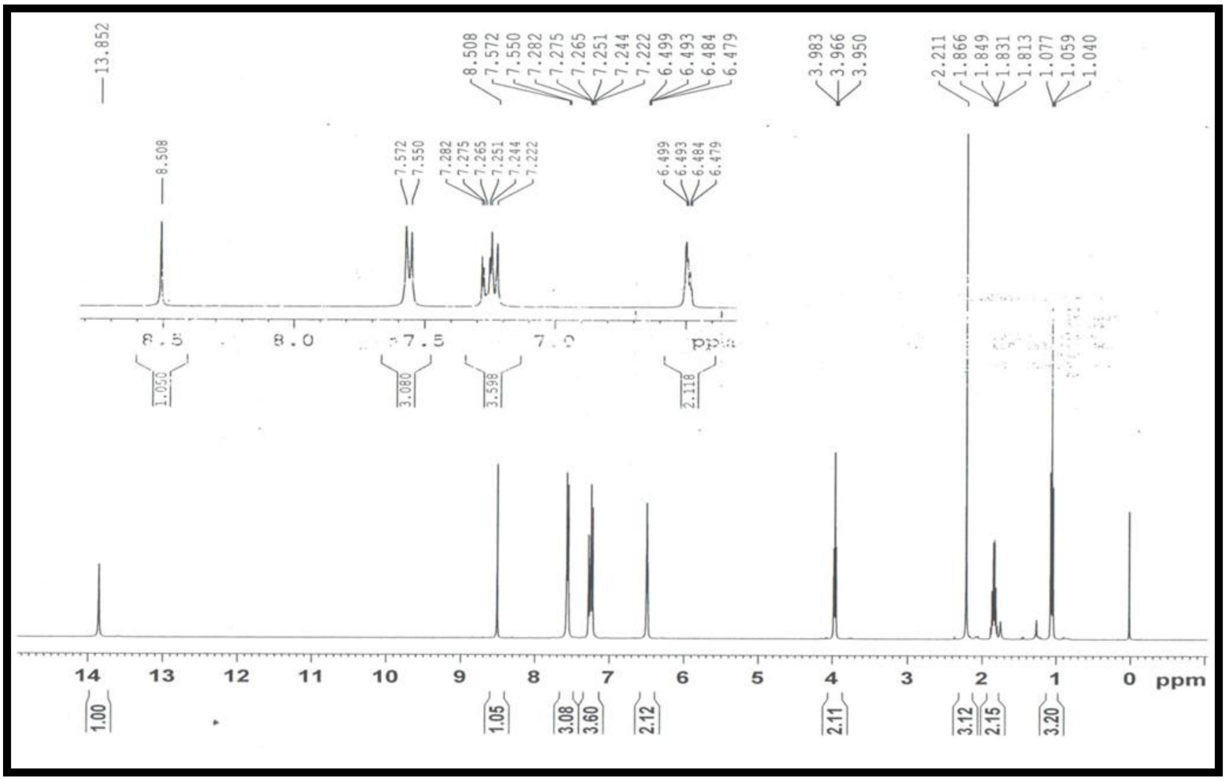

[1]H NMR of C3

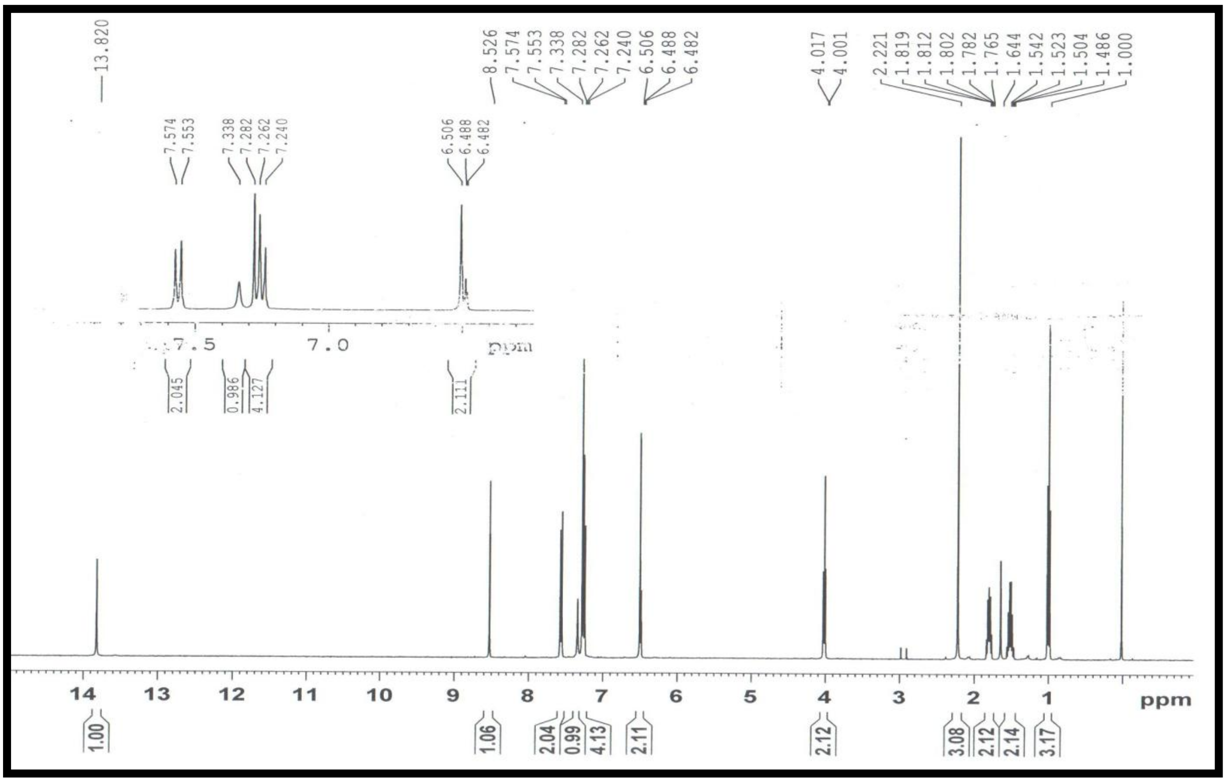

[1]H NMR of C4

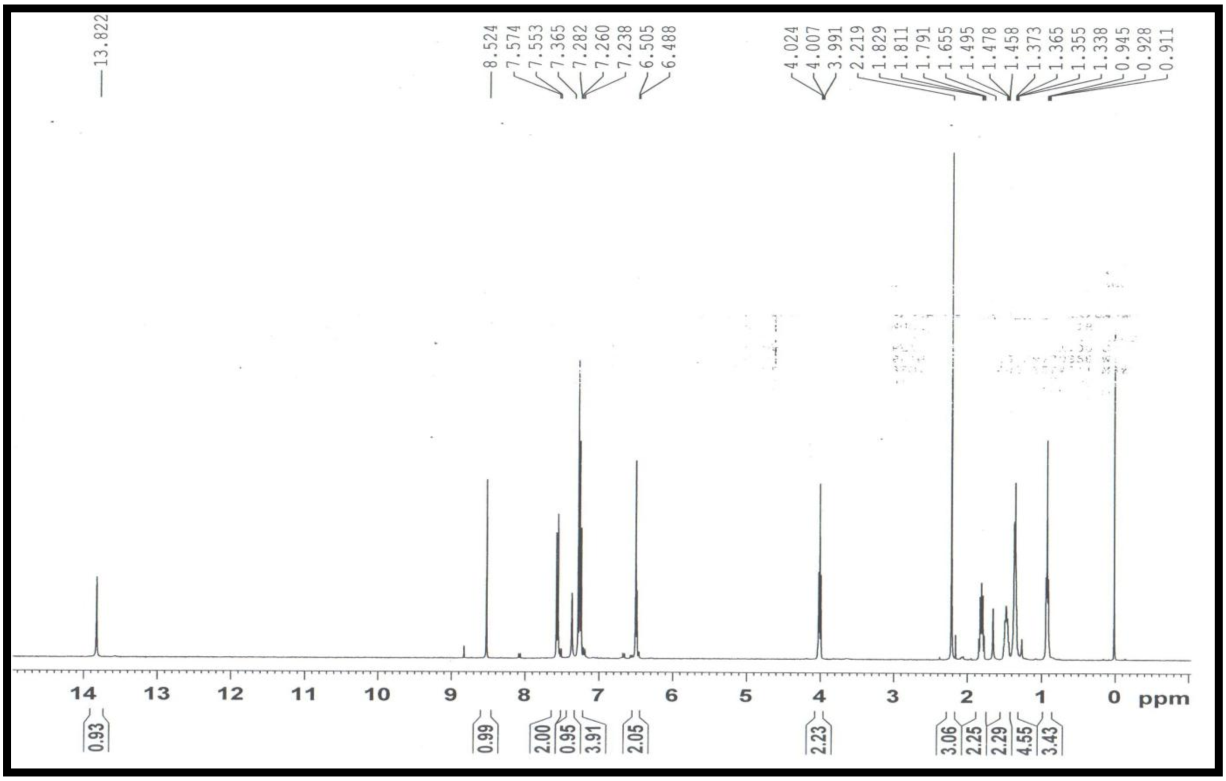

^{1}H NMR of C6

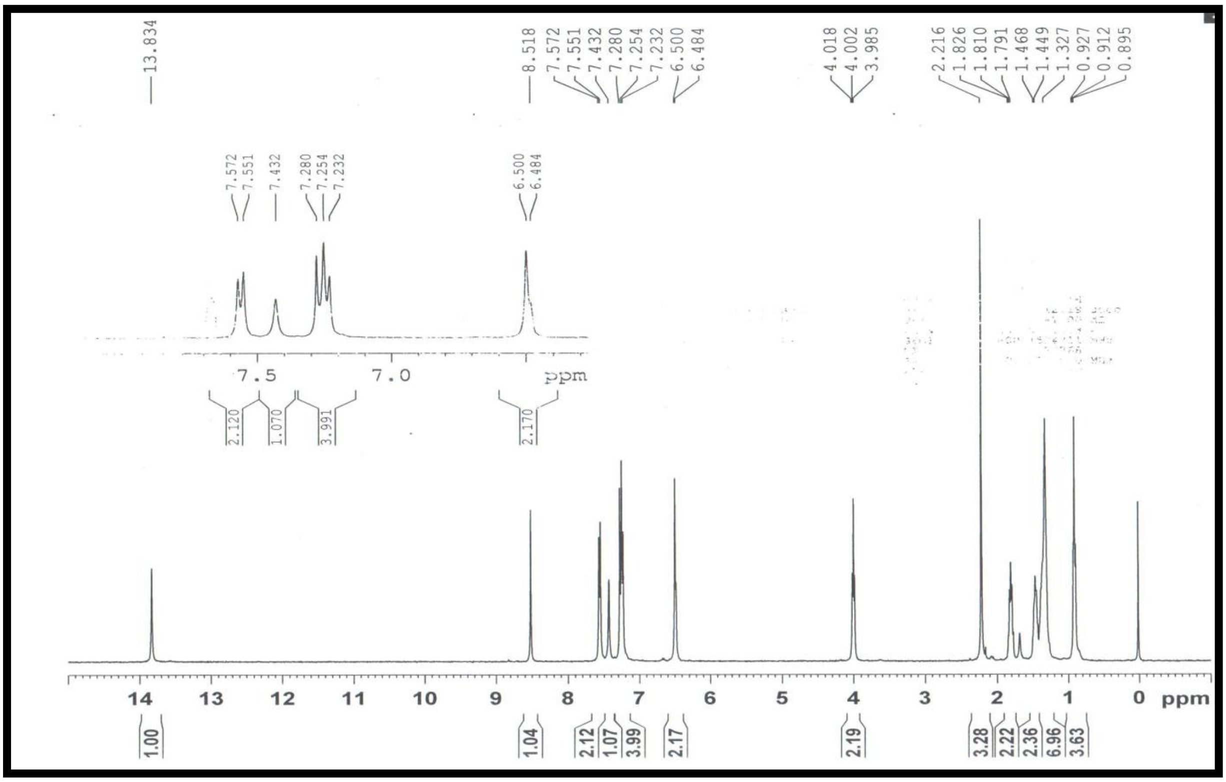

^{1}H NMR of C7

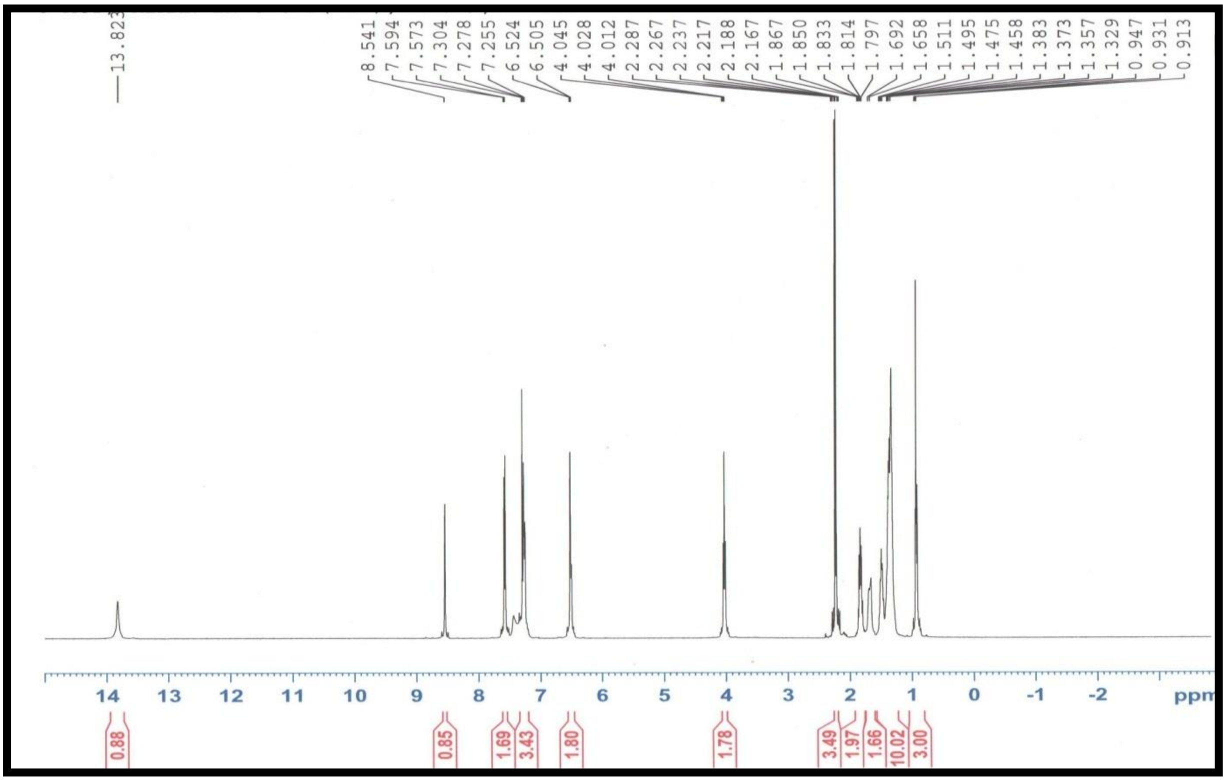

[1]H NMR of C8

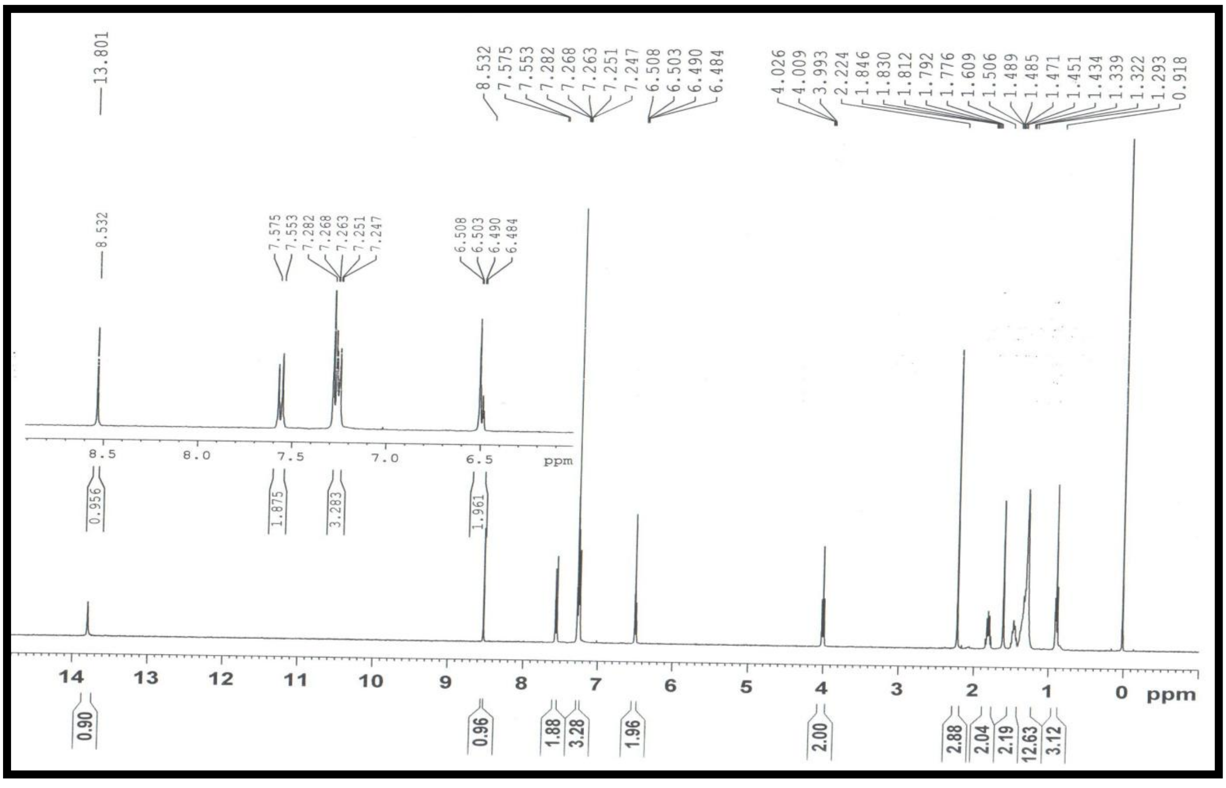

[1]H NMR of C10

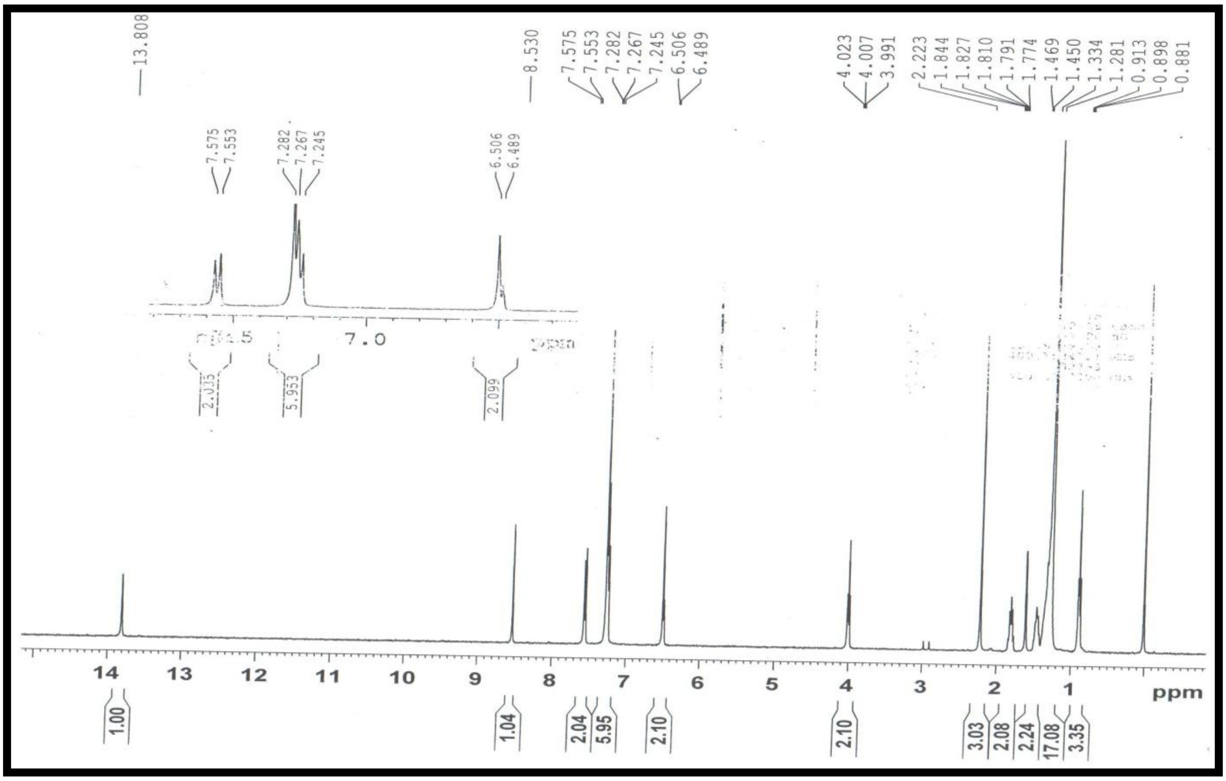

^{1}H NMR of C12

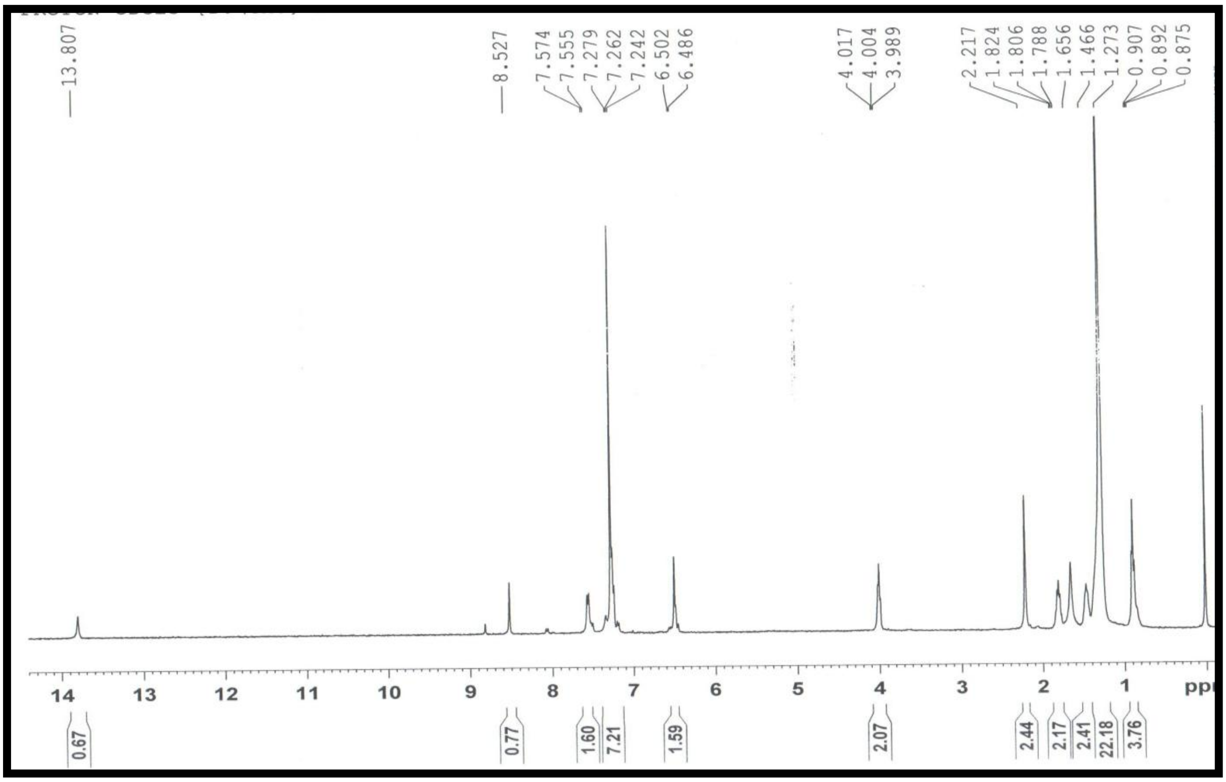

^{1}H NMR of C14

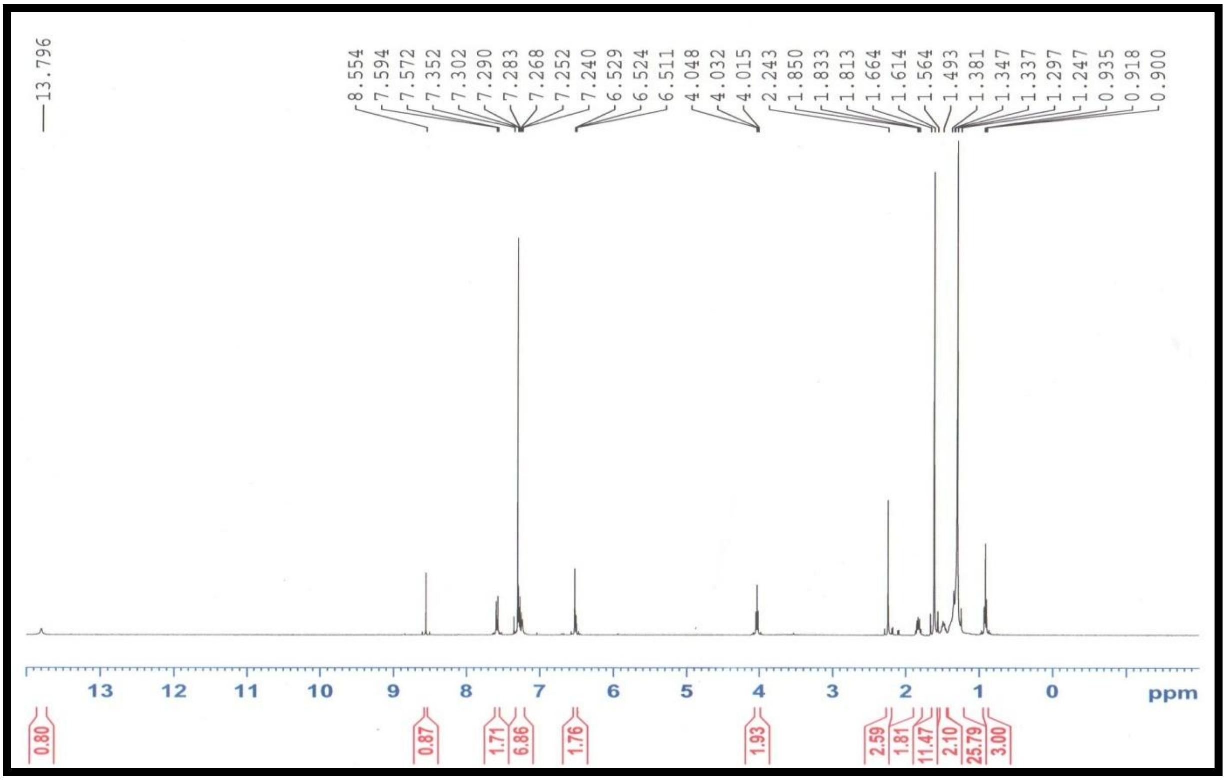

[1]H NMR of C16

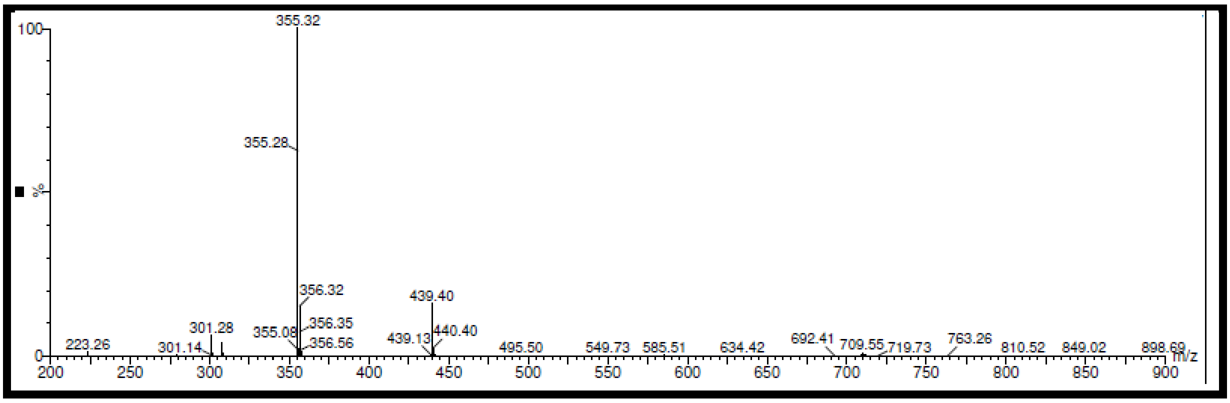

Mass spectra of C6

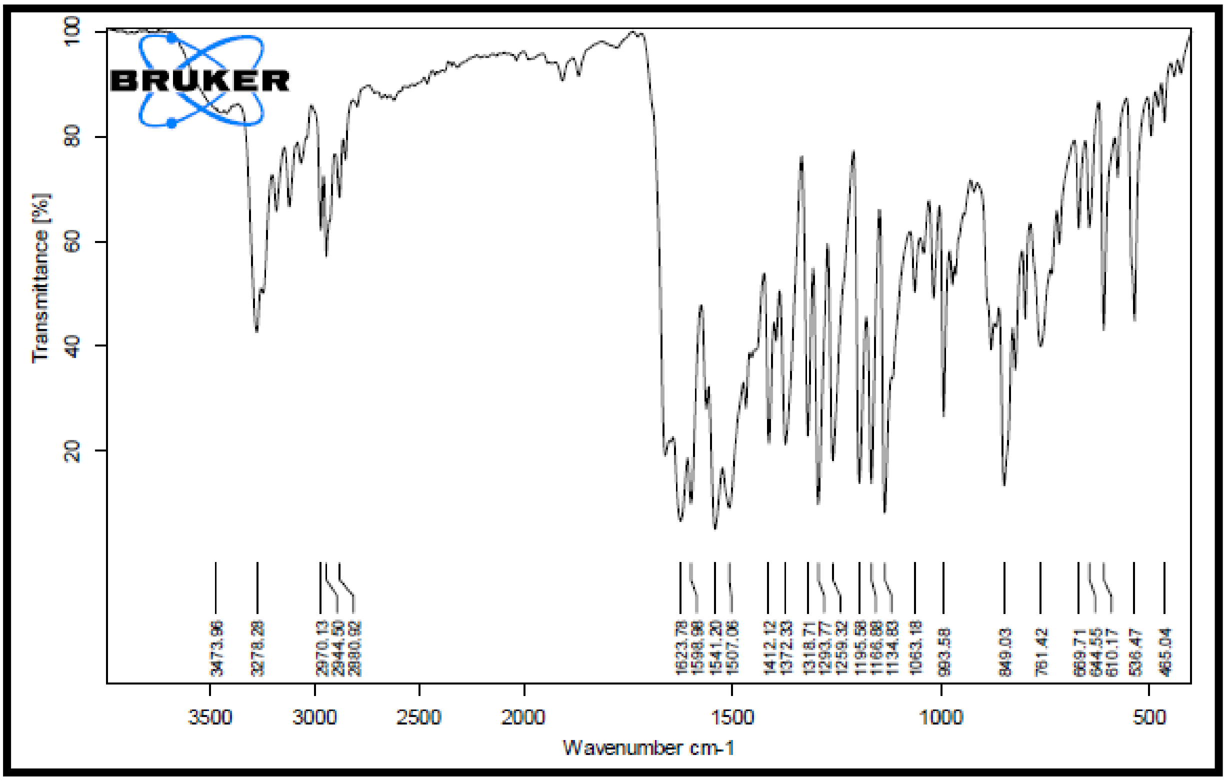

IR spectra of C3

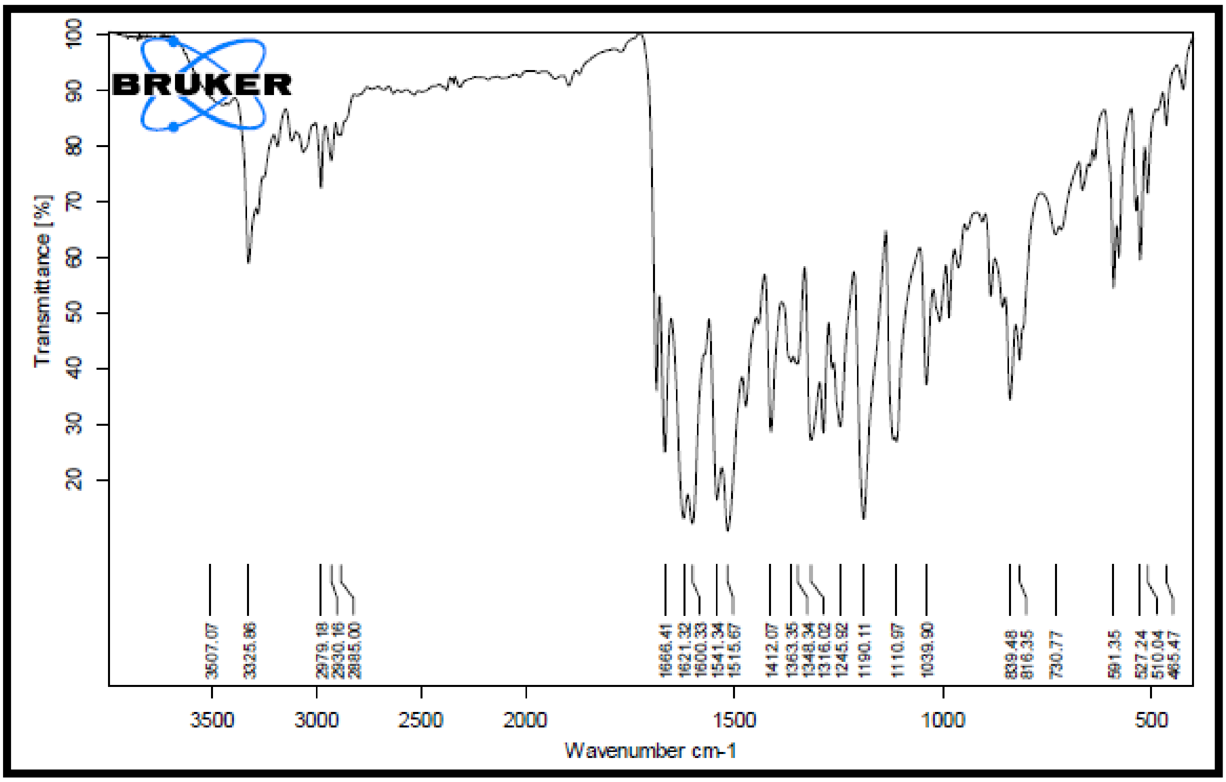

IR spectra of C4

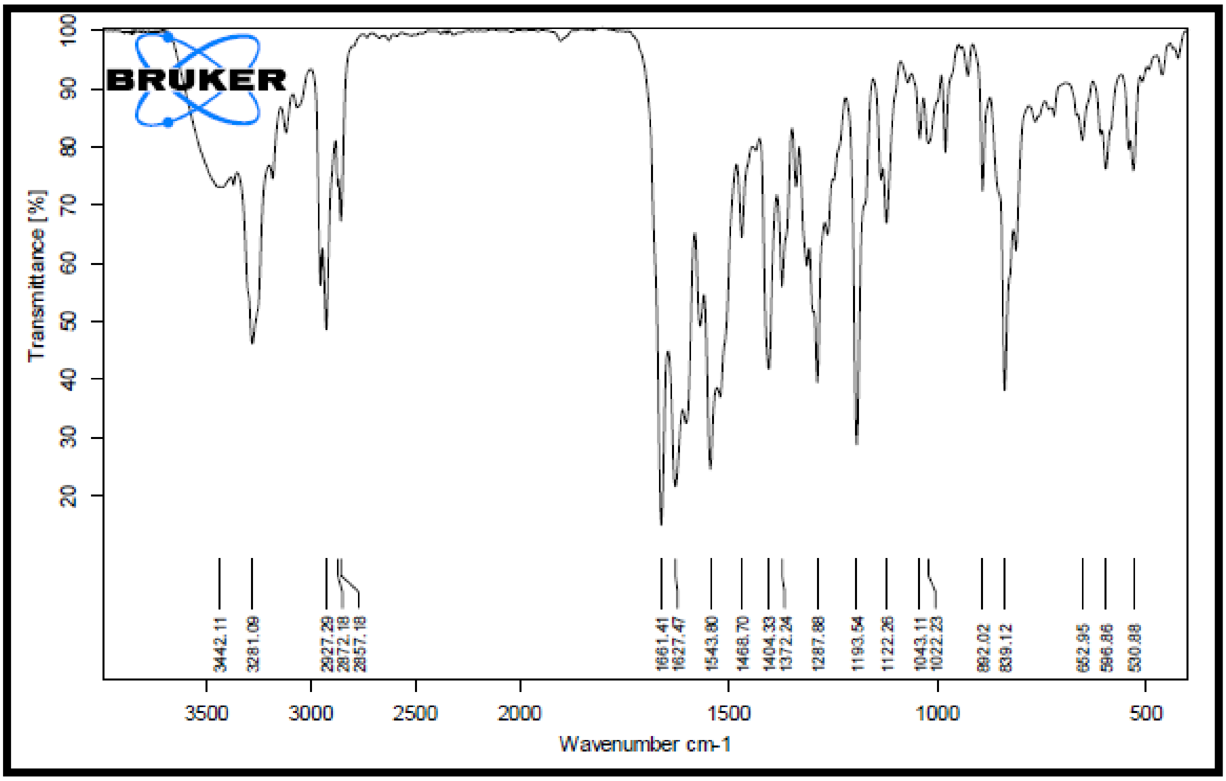

IR spectra of C6

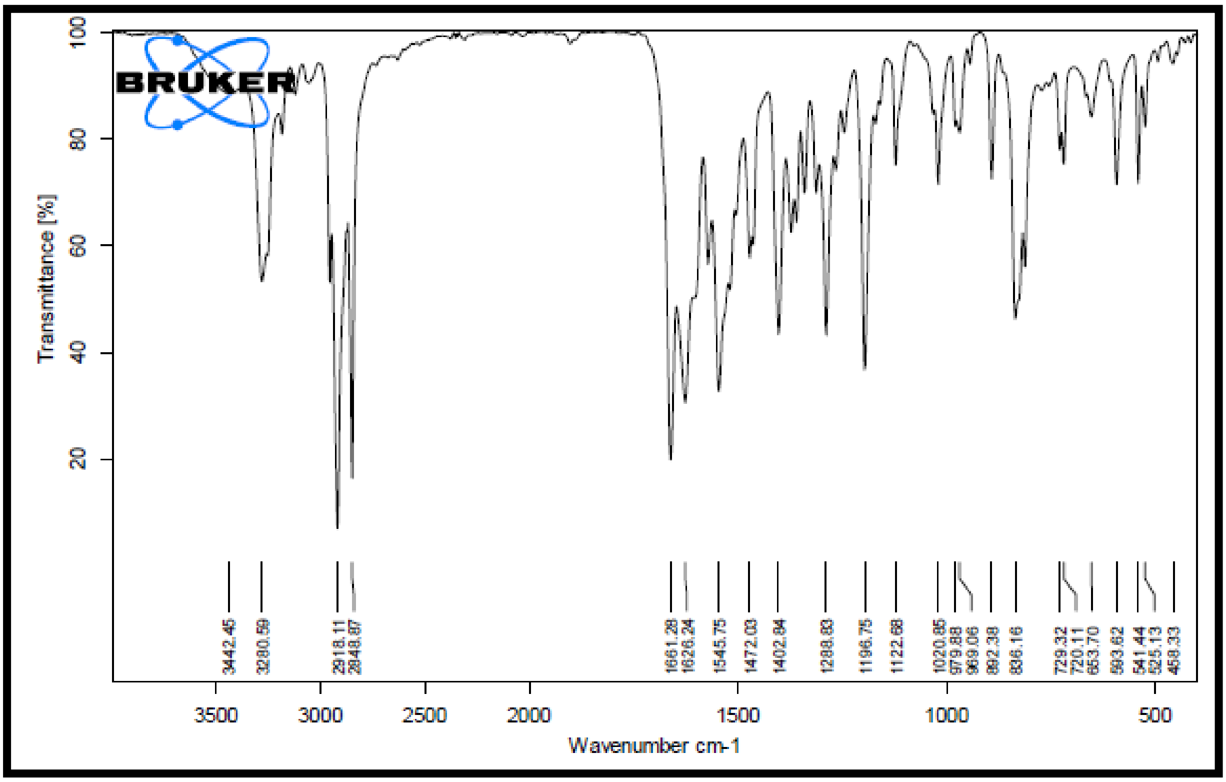

IR spectra of C7

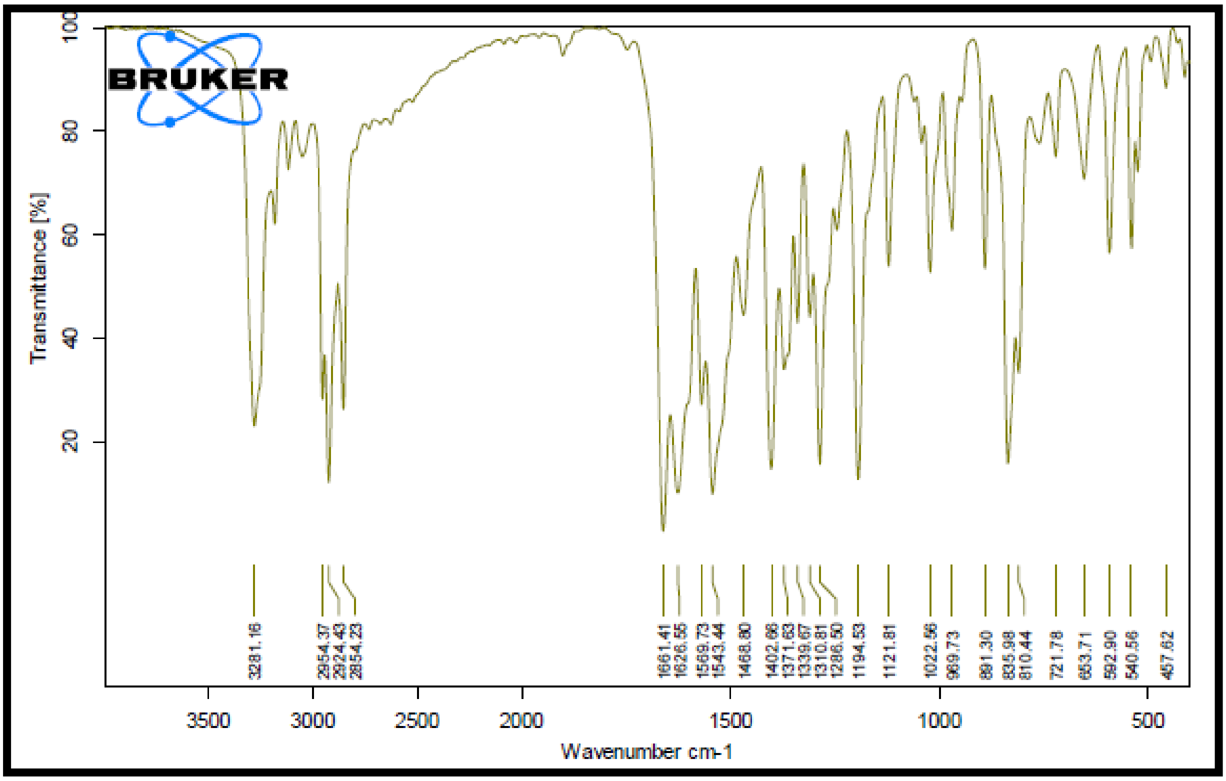

IR spectra of C8

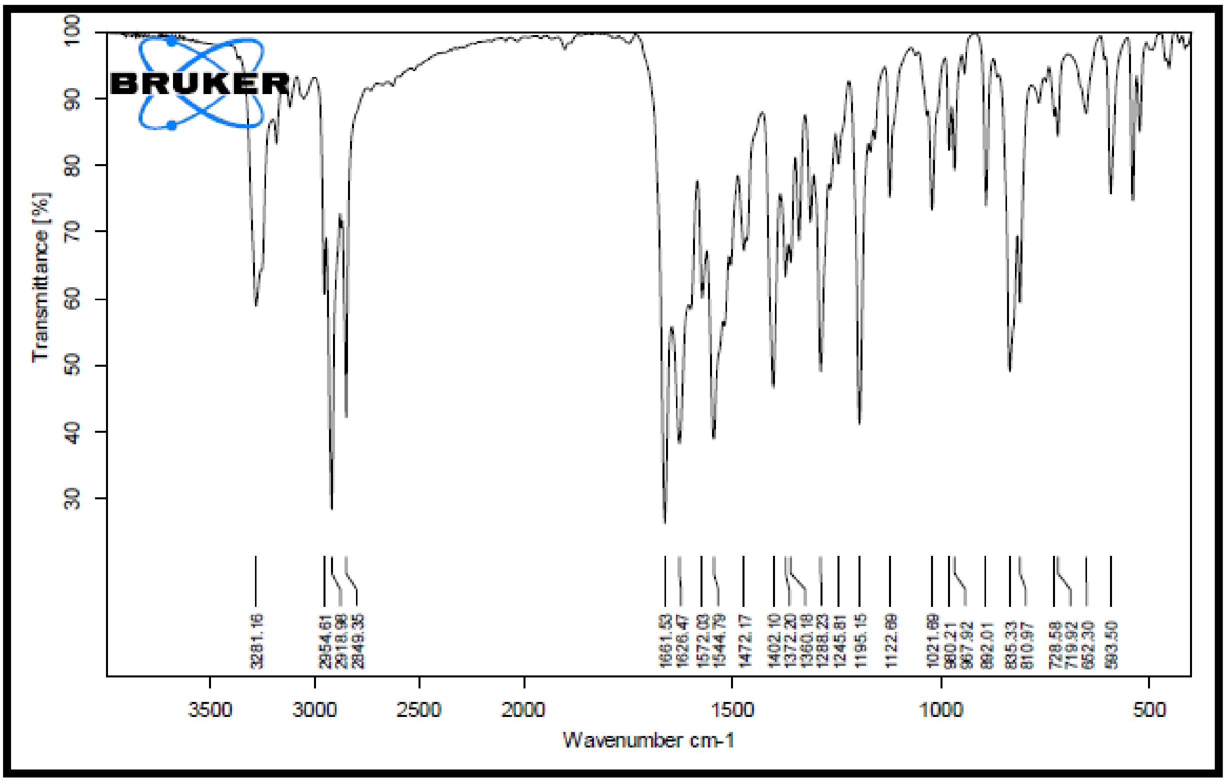

IR spectra of C10

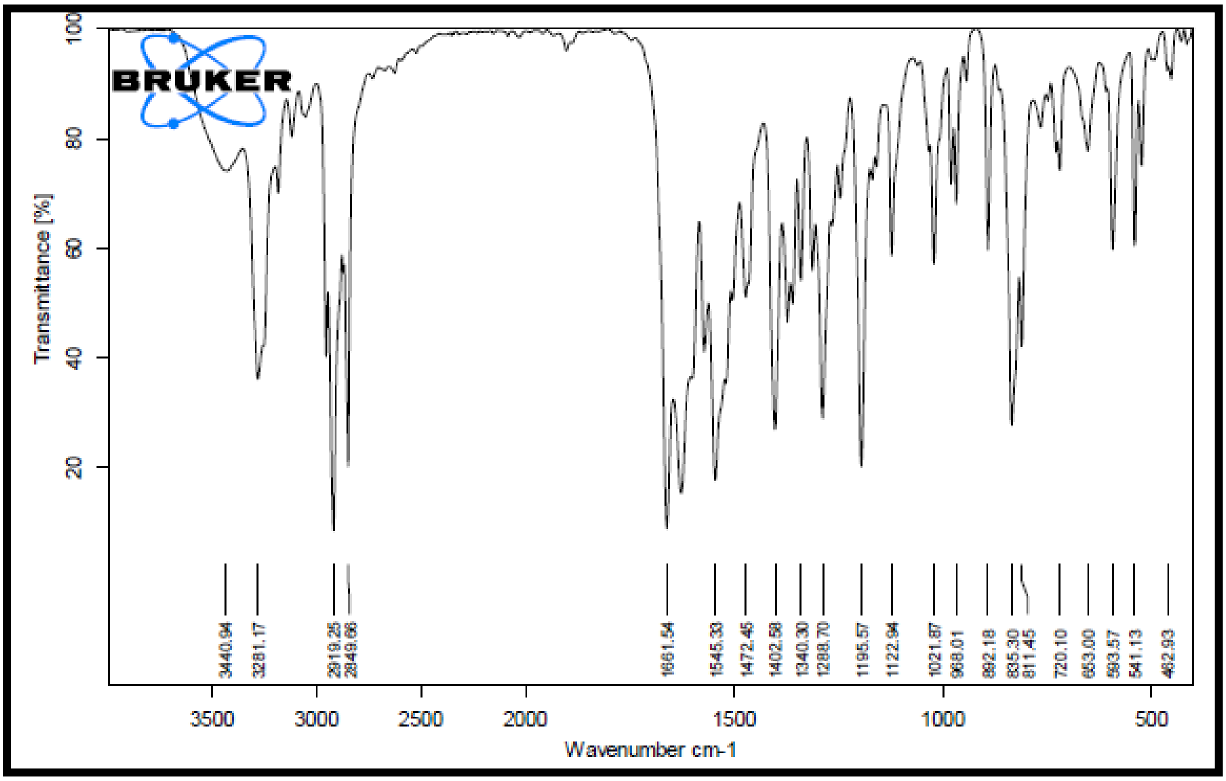

IR spectra of C12

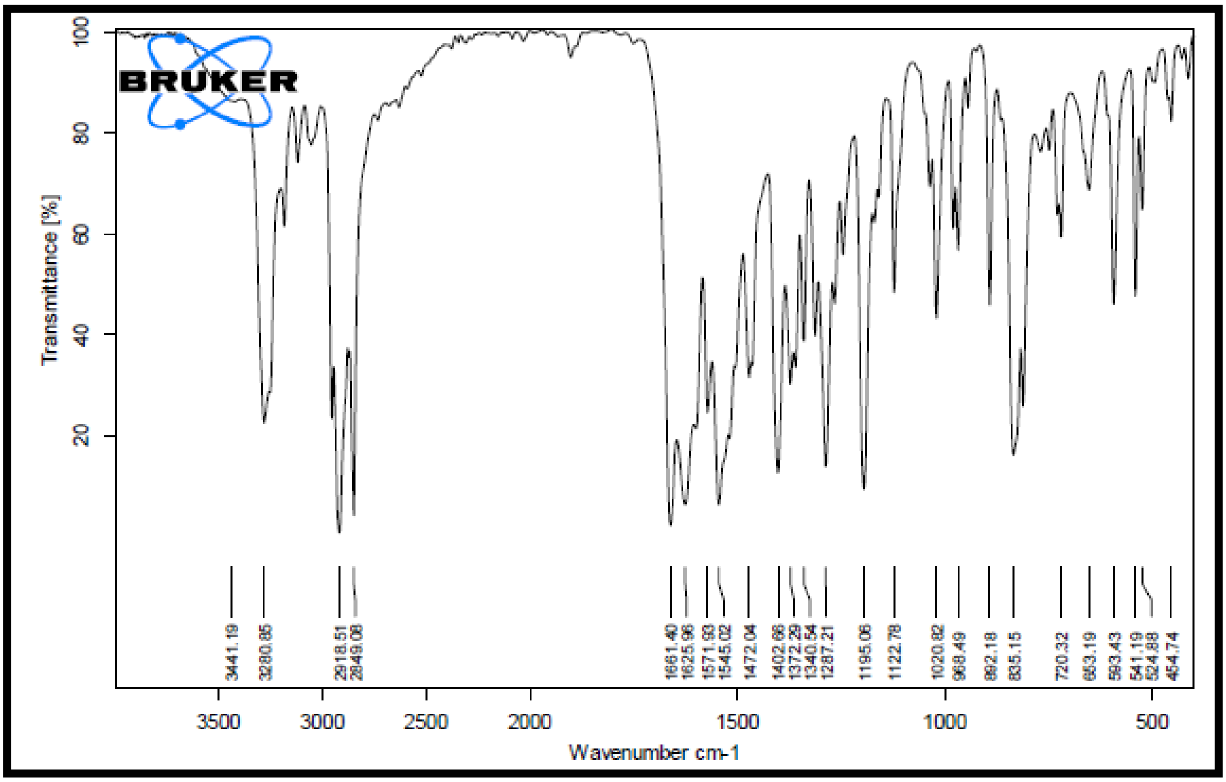

IR spectra of C14

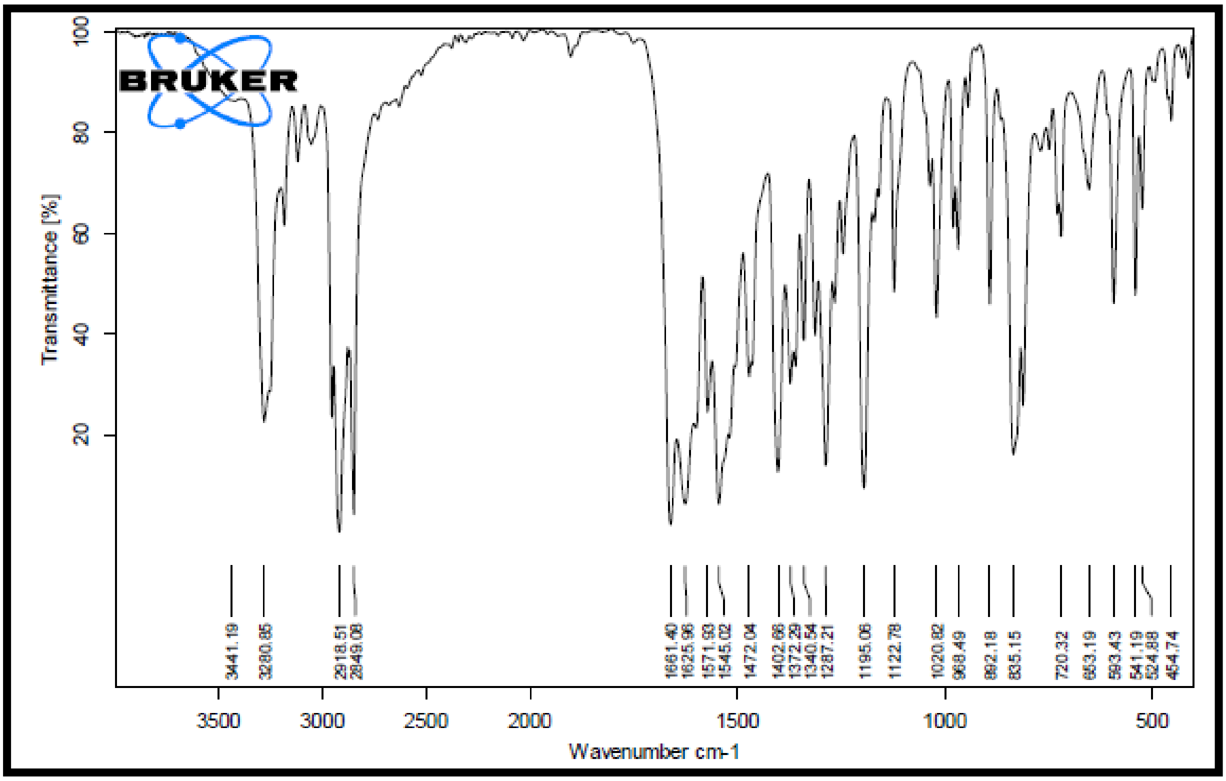

IR spectra of C16

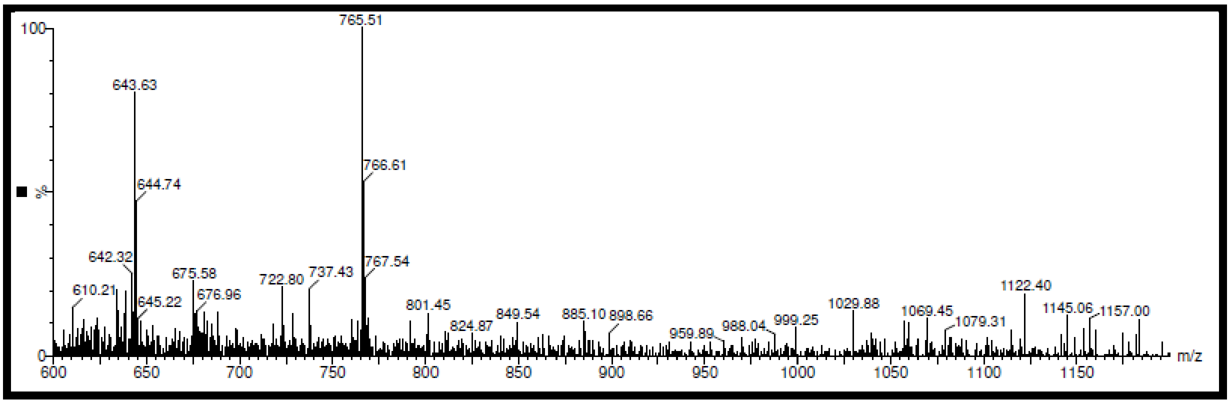

Mass spectra of D6

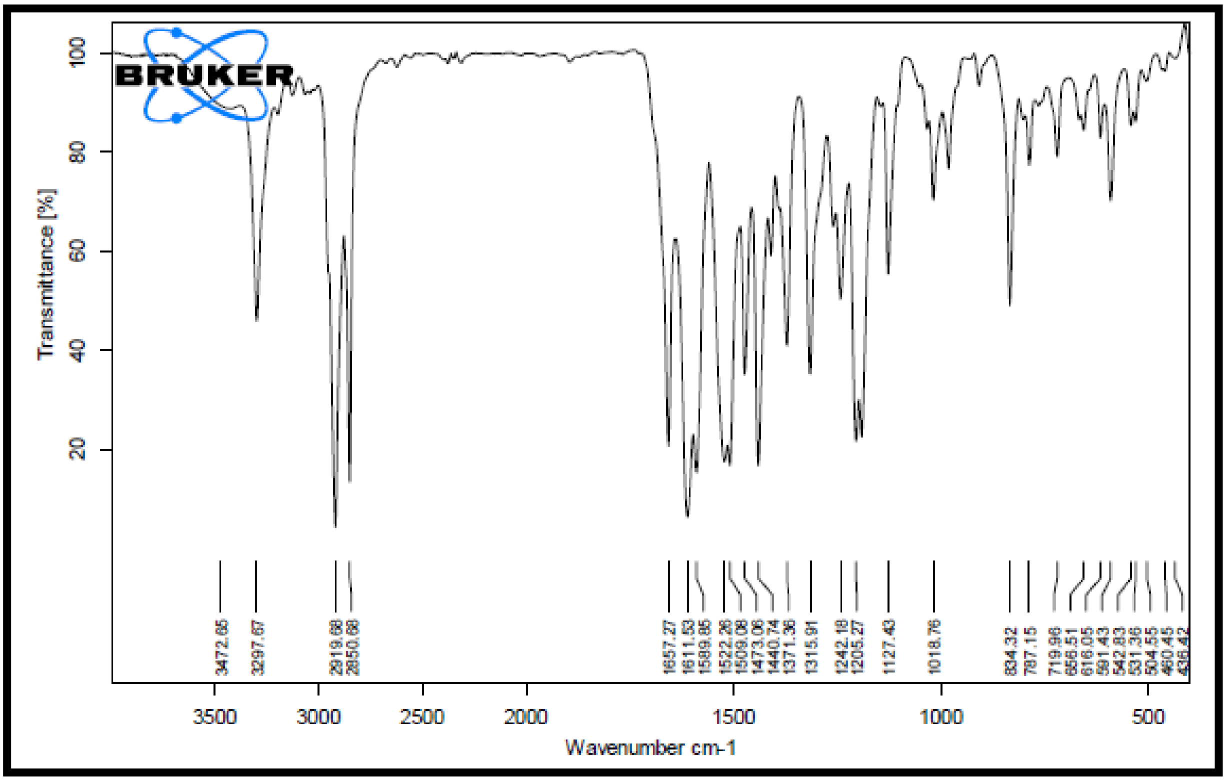

IR spectra of D4

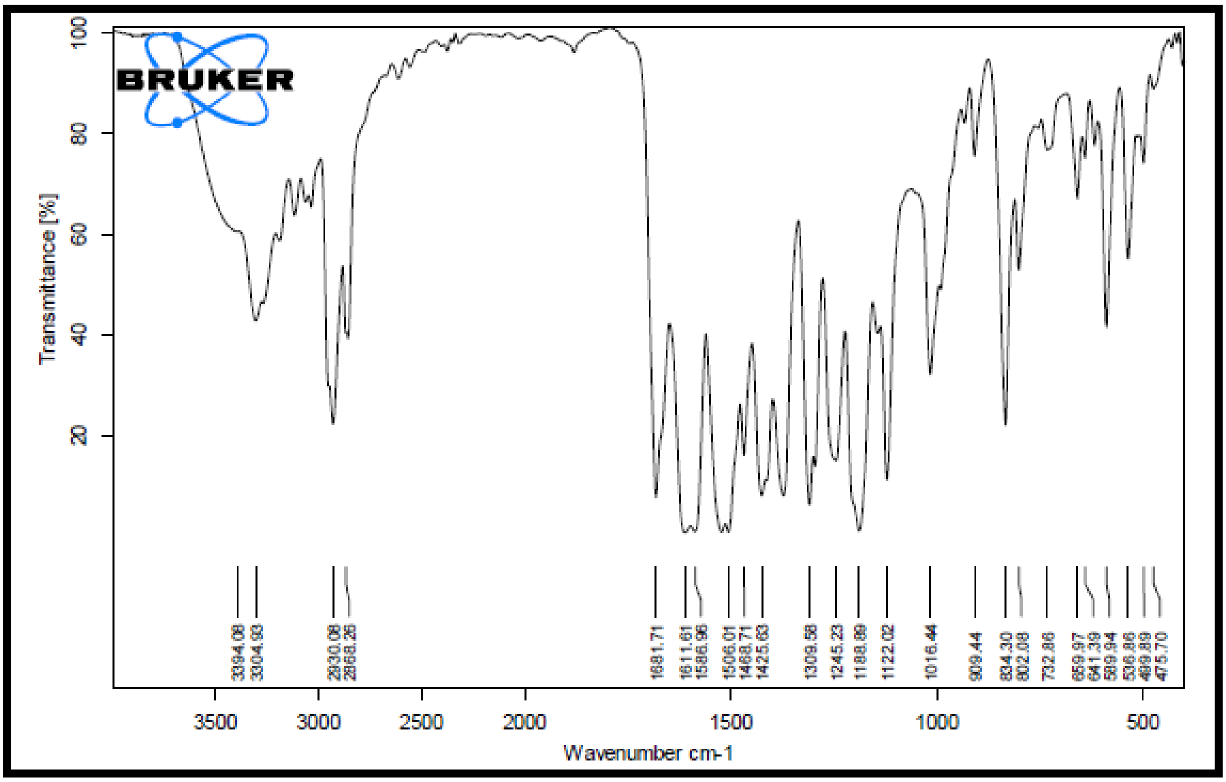

IR spectra of D6

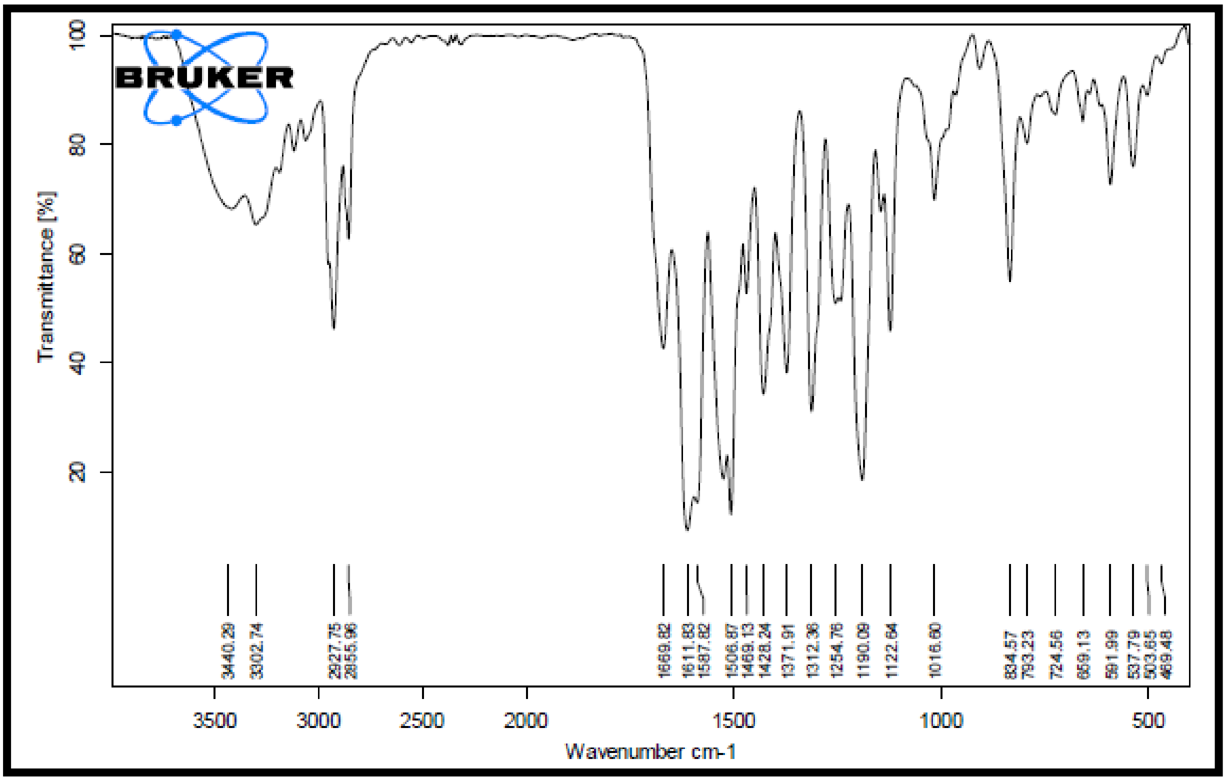

IR spectra of D7

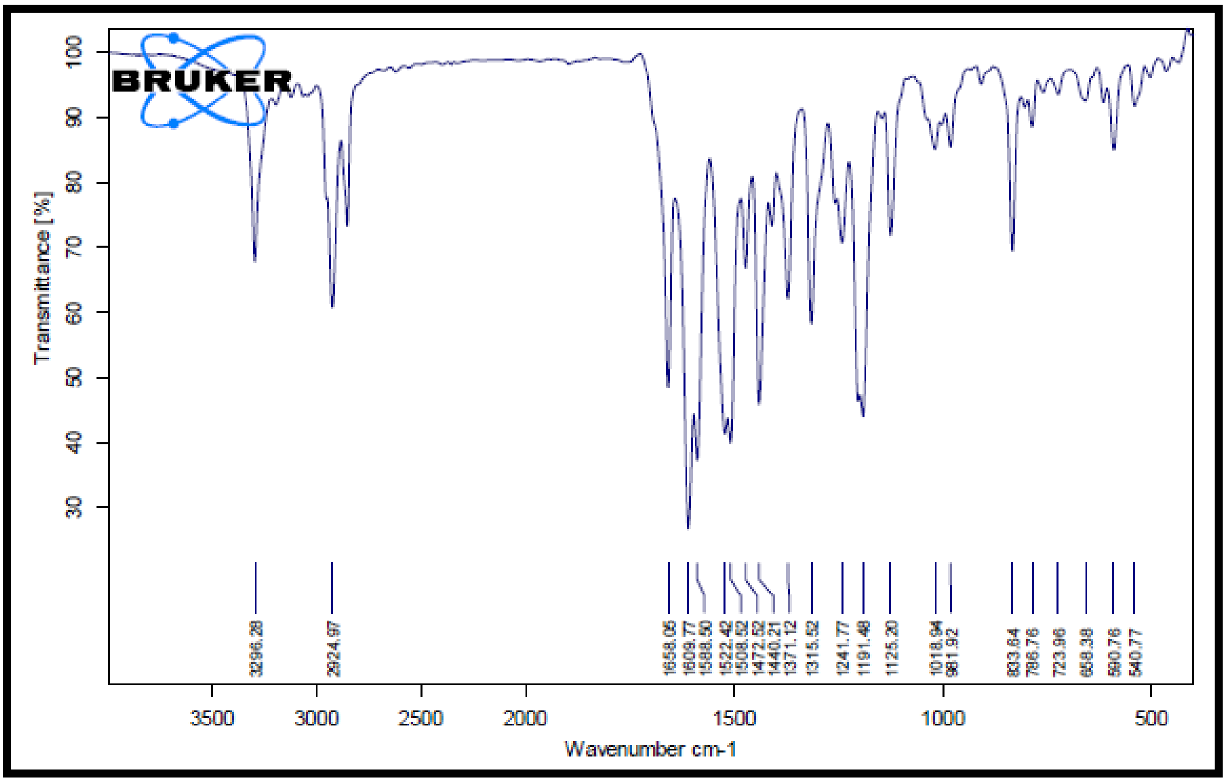

IR spectra of D8

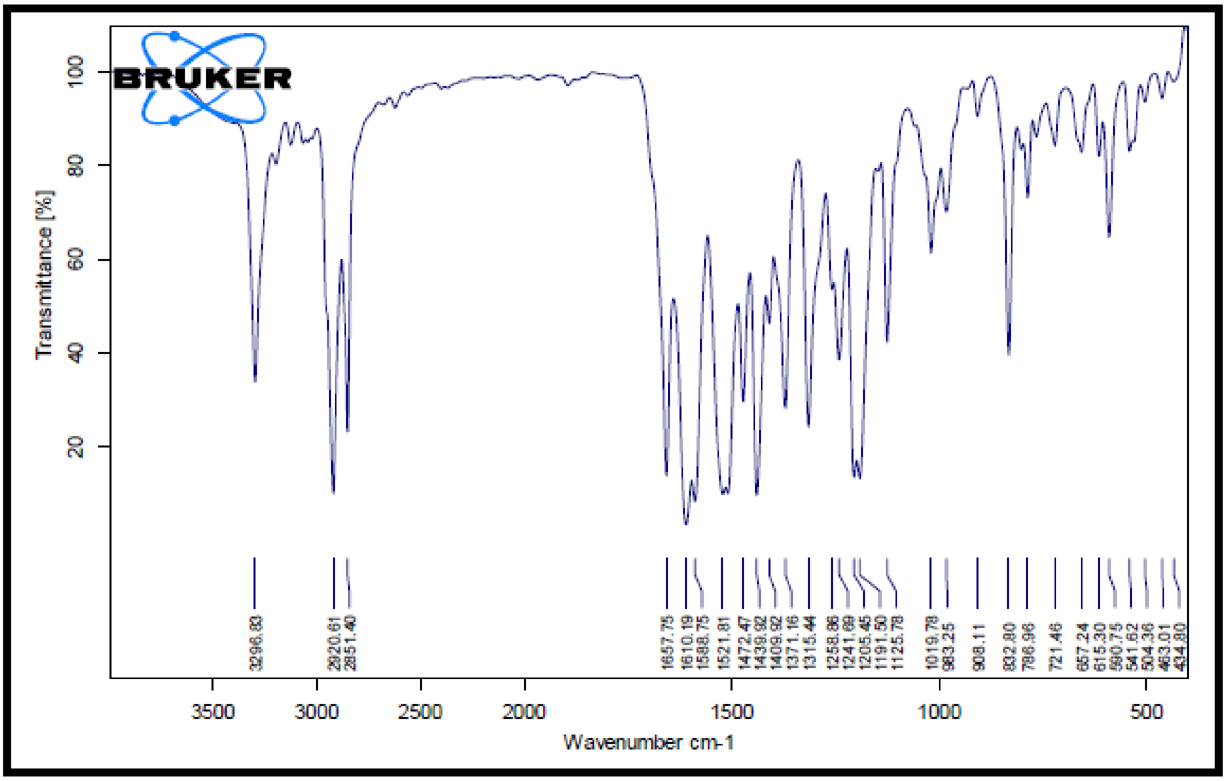

IR spectra of D10

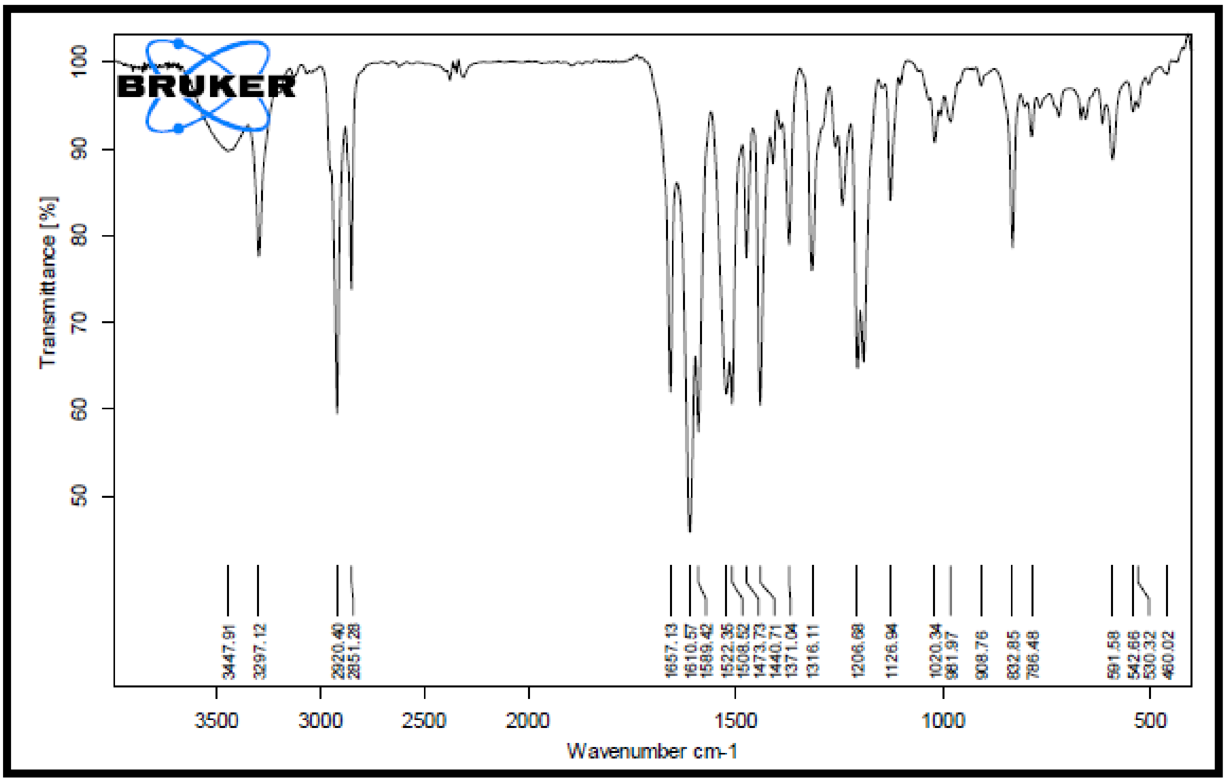

IR spectra of D12

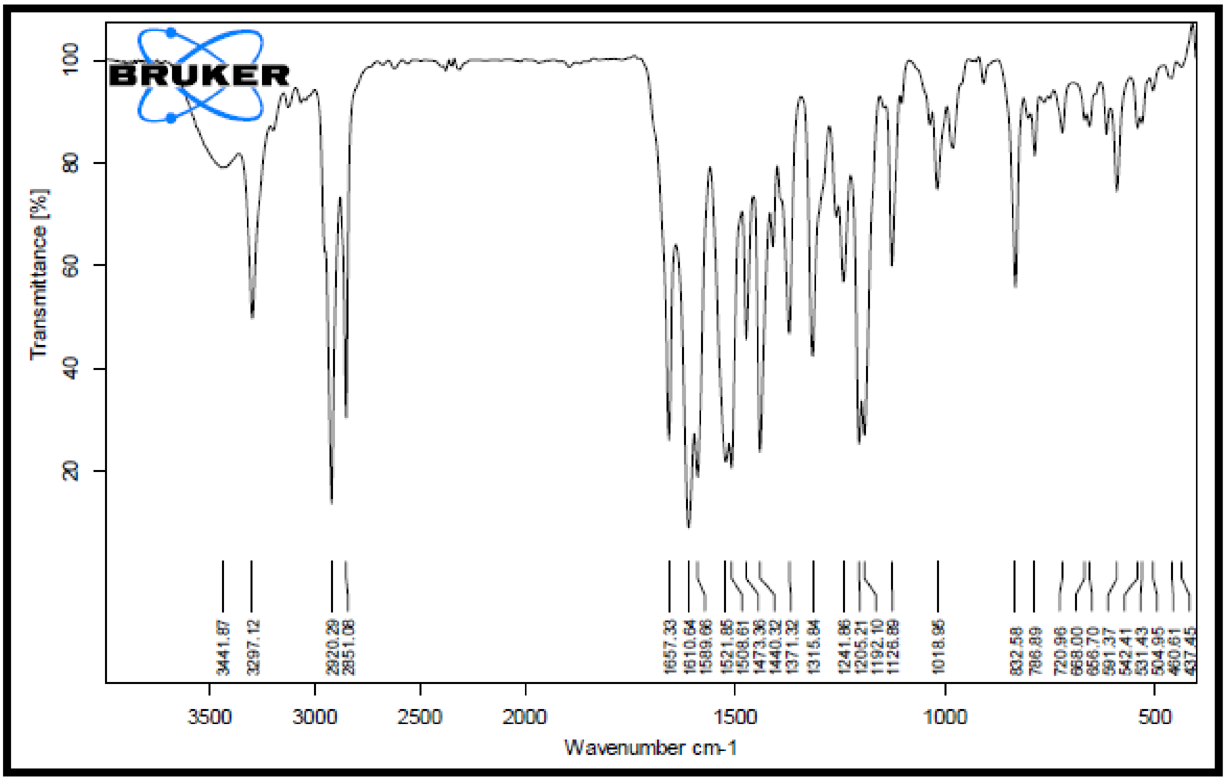

IR spectra of D14

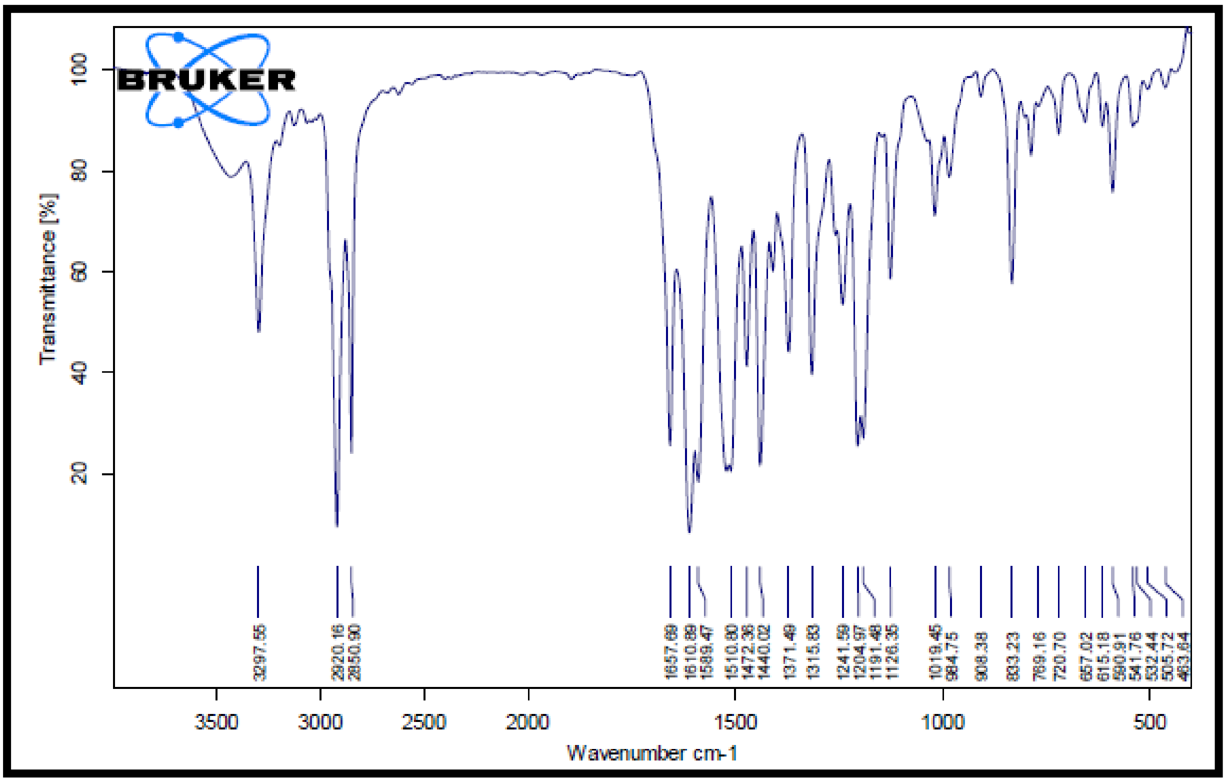

IR spectra of D16